T H E U N I V E R S I T Y O F T U L S A

THE GRADUATE SCHOOL

GAS WELL LIQUID LOADING ONSET AND PLUNGER LIFT MODELING

by
Weiqi Fu

A thesis submitted in partial fulfillment of

the requirements for the degree of Master of Science

in the Discipline of Petroleum Engineering

The Graduate School

The University of Tulsa

2016

T H E U N I V E R S I T Y O F T U L S A

THE GRADUATE SCHOOL

GAS WELL LIQUID LOADING ONSET AND PLUNGER LIFT MODELING

by
Weiqi Fu

A THESIS

APPROVED FOR THE DISCIPLINE OF

PETROLEUM ENGINEERING

By Thesis Committee

_____, Chair
Holden Zhang

_____
Eduardo Pereyra

_____
Junqi Wang

ABSTRACT

Weiqi Fu (Master of Science in Petroleum Engineering)

Gas Well Liquid Loading Onset and Plunger Lift Modelling

Directed by Holden Zhang

114 pp., Chapter 6: Summary, Conclusions and Recommendations

(200 words)

Based on the Zhang et al. (2003) unified model, liquid loading behavior in gas wells is studied in this thesis. The predictions of liquid loading are analyzed for different well inclinations including 90°, 75° and 60°. Superficial liquid velocities of 0.01, 0.05 and 0.1 m/s are selected for comparison. The minimum pressure gradient and liquid film velocity reversal concepts are examined as liquid loading onset criteria in gas wells. Compared with experimental data of Yuan (2011), the liquid film velocity reversal method gives better predictions of liquid loading for the studied well inclination angles.

A plunger lift mechanistic model is developed to simulate the plunger lift working process and predict the production rates in gas wells with plunger lift operation. The model is based on the approaches presented by Lea (1982) and Gasbarri and Wiggins (2001). Improvements have been made on the equations of plunger rising and falling velocities. The present model also accounts for different reservoir performances in plunger lift simulation. Oil and water cases from previous studies are used to evaluate the present model which provides more accurate and reasonable predictions of plunger rising

and falling velocities. Further validations of this model are recommended when more field data become available.

ACKNOWLEDGEMENTS

I would like to express my sincere gratitude to my academic advisor, Dr. Holden Zhang, for giving me continuous support, guidance, and encouragement throughout my graduate study. His personal and professional encouragements helped me face challenges in my study and life. I feel very proud to be his student.

I would like to thank Dr. Zhiyuan Wang, visiting scholar from China University of Petroleum (East China), for his great assistance through this project. I am honored and fortunate to have worked with him.

I appreciate Dr. Eduardo Pereyra and Dr. Junqi Wang for being on my thesis committee and for their technical inputs.

Thanks to our very friendly and resourceful TUALP staff Donna Trankley and Bryan Sams. My sincere thanks go to Jianjun Zhu, Haiwen Zhu, Dr. Hongfang Gu, Jiecheng Zhang and Yuchen Ji, for their assistance and encouragement in my research and study.

Finally, I would like to dedicate this thesis to my beloved family: my parents Jianjun Fu and Hua Wei, my grandfather, Xiaoyu Wei. I thank them from my heart for their emotional and financial support for my bachelor and master studies. Their endless love and support have allowed me to finish my study in the United States. Their continuous encouragement and guidance help me continue the journey of my life.

TABLE OF CONTENTS

LIST OF FIGURES

LIST OF TABLES

INTRODUCTION

Normally, natural gas production is accompanied with liquid production or liquid condensation. At high gas production rates, gas flow can carry liquid phase to the surface. With continuous production, reservoir pressure will decrease due to reservoir depletion which leads to gas flow rate decreasing. When gas production rate decreases, its ability to carry liquid upward will weaken due to its kinetic energy decrease. Therefore, a critical gas flow rate exists, below which gas is unable to carry all liquid phase to the surface and thus liquid begins to accumulate at the bottom of wells. Natural gas production decreases further and even stops due to liquid accumulation in the wellbore. This phenomenon, termed as liquid loading, commonly occurs in gas wells accompanied by flow regime transitions shown in Figure 1.

In order to avoid liquid loading and maintain gas production rate, the onset of liquid loading in gas wells needs to be predicted. Many researchers have proposed methods to predict liquid loading in gas wells. One of the earliest models was proposed by Turner et al. (1969) and is probably the most popular model for liquid loading prediction. Later, this model was modified by several studies including Guo et al. (2005) and Zhou et al. (2009). The Turner et al. model provides a general equation to calculate the critical gas flow rate, which can be used to determine whether liquid loading occurs or not in gas wells.

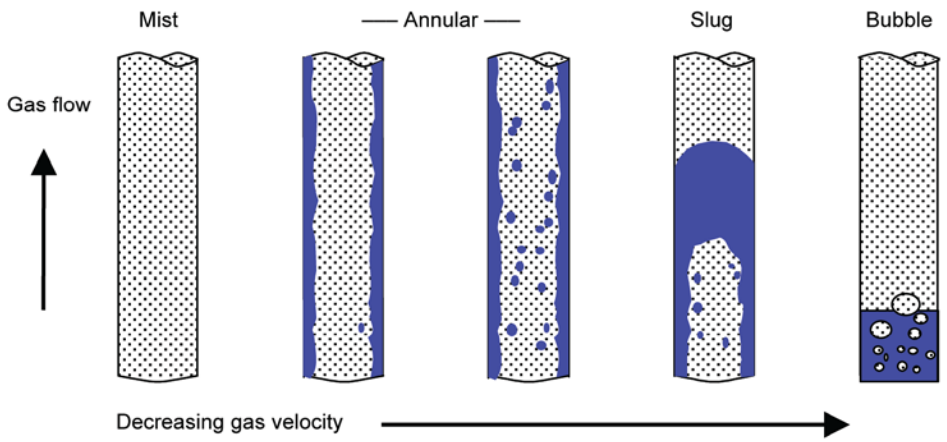

Figure 1: Gas Well Liquid Loading Flow Patterns

(http://petrowiki.org/Plunger_lift)

Mechanistic multiphase flow models, such as Barnea et al. (1987) model and Zhang et al. (2003) unified model, can be used to analyze liquid loading in gas wells. The liquid film reversal and minimum pressure gradient are believed to relate to the onset of liquid loading. Yuan (2011) and Gunner (2012) conducted pertinent experimental measurements and analyzed mechanistic model predictions. In this study, liquid loading in gas wells is predicted by the Zhang et al. unified model, and liquid loading mechanism is analyzed for different gas well inclinations including 90°, 75° and 60°.

Artificial lift methods can be used to unload liquid from gas wells, among which plunger lift are an effective approach (as shown in Figure 2). Plunger lift has many advantages such as lower operation cost, prevention of paraffin deposition along wellbore and easy to manage. For low productivity oil wells with high gas-liquid ratio and some old oil wells, plunger lift is also preferred due to its low cost of maintenance and work over.

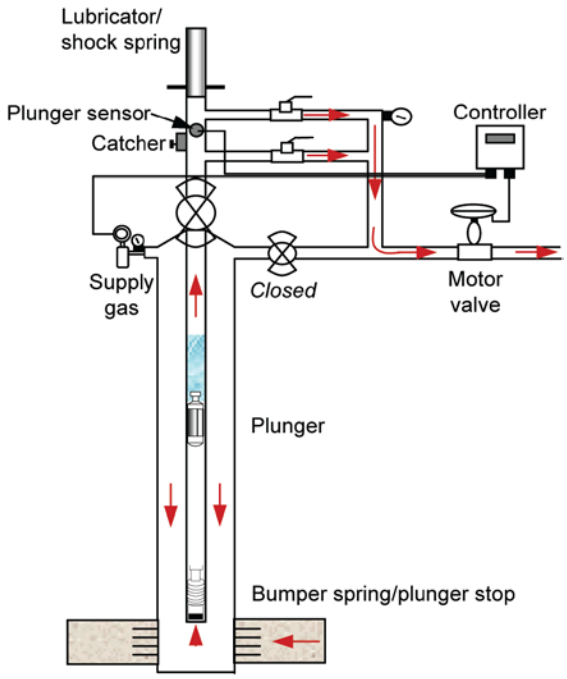

Figure 2: Plunger Lift System

(http://petrowiki.org/Plunger_lift_installation_and_maintenance)

For decades, several plunger lift models have been developed. The first model for plunger lift proposed by Foss and Gaul (1965) was a static model, based on which a dynamic model was first presented by Lea (1982). Mower and Lea (1985) conducted experiments to evaluate several assumptions made in the Foss and Gaul model. Thereafter, a new plunger lift model treating liquid fallback during the plunger moving upward was proposed by Marcano and Chacín (1994). A more recent plunger lift model was proposed by Gasbarri and Wiggins (2001) with consideration of gas sections above and below the plunger. A plunger lift simulator was developed by Gasbarri and Wiggins using Fortran programming language.

The existing models are still imperfect due to individual limitations or assumptions with which the models were simplified to a great extent. The models can be improved if the following aspects can be taken into account:

- Most of the existing models take the plunger rising velocity and falling velocity as constant.
- The prediction of liquid loading onset in plunger lift modeling is unavailable.
- Few of the existing models have been implemented successfully into plunger lift simulator.
- The lack of field data impedes the development of more accurate plunger lift models.

In this study, a new model will be developed considering changes of plunger rising and falling velocities, as well as liquid loading prediction. In this study, a new plunger model with these considerations is proposed, based on which ~~a~~ plunger lift simulator is developed. In addition, the liquid loading onset criteria in gas wells are compared with available experimental data.

CHAPTER 1

LITERATURE REVIEW

In order to prevent liquid loading in gas wells, it is important to predict liquid loading onset. The understanding of the fundamental mechanism that triggers liquid loading in gas wells is needed to develop accurate prediction models.

As an efficient method to keep gas wells from liquid loading, plunger lift has been widely used in fields. In this study, a new plunger lift model is developed with further improvement of previous models. Thus, a literature review of liquid loading prediction and existing plunger lift models has been conducted.

1.1 Liquid Loading Prediction

Since 1969, several liquid loading prediction methods have been proposed, which can be classified into two categories: correlation and mechanistic model. The first correlation was proposed by Turner et al. (1969), who analyzed force balance on liquid droplets in vertical gas flow and obtained a critical gas flow rate to determine liquid loading in gas wells. Initially, Turner et al. model was only applied to vertical gas wells. However, researchers later extended this model to deviated wells and improved the accuracy of the original model with necessary modifications and additional correlations.

The mechanistic methods for liquid loading prediction in gas wells originate from mechanistic multiphase flow models, such as Barnea (1987) model and Zhang et al.

(2003) unified model, which are used to predict multiphase flow behavior in pipeline and wellbore. The liquid film velocity and pressure gradient predicted by mechanistic models can be used as the criteria to determine liquid loading in gas wells.

1.1.1 Correlations

Correlations for predicting liquid loading onset include the Turner et al. (1969) model and the models developed from Turner et al. model by other researchers. Turner et al. model is widely used to predict liquid loading onset in gas wells by industry, because it is a straight forward correlation. However, due to its simplicity, Turner et al. model can only be applied in vertical wells, and the prediction results have larger discrepancies compared with field data. Thereafter, researchers including Guo et al. (2005) and Zhou et al. (2009), improved Tuner et al. model by incorporating new correlations or accounting more parameters in modeling such as liquid holdup and kinetic energy.

Turner et al. (1969) claimed that liquid loading in the vertical wells is due to liquid droplets falling downward. The terminal velocity, also called the critical gas flow velocity, is derived based on force balance of gravity and drag force on liquid droplets sustained by gas flow (Figure 3). It is the minimum gas velocity required to carry all liquid droplets upward. The general form of terminal velocity equation is given as:

$$v_t = 17.6 \frac{\sigma_L^{1/4} \left(\rho_L - \rho_G\right)^{1/4}}{\rho_G^{1/2}} \qquad 2.1$$

Where v_t is terminal velocity, ft/s, σ_L is liquid gas interfacial tension, dynes/cm, ρ_L is liquid density, lb_m/ft^3 and ρ_G is gas density, lb_m/ft^3.

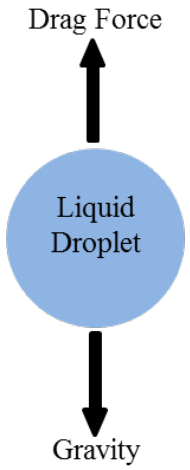

Figure 3: Liquid Droplet Force Balance

Turner et al. (1969) used field data, including 101 wells with most wellhead pressures above 500 psig, to validate the droplet entrainment model. It was pointed out that prediction results require a 20% upward adjustment to match field data. Turner et al. believed that the liquid droplet entrainment was the main mechanism controlling liquid loading in gas wells while the liquid film reversal mechanism is unimportant.

Coleman (1991) used EXXON field data with wellhead pressures less than 500 psig to validate the Tuner et al. (1969) model. He concluded that 20% upward adjustment of the Turner et al. model was unnecessary based on his assessment. Coleman also pointed out that wellbore size and wellhead pressure affected terminal velocity of liquid droplets significantly. However, gas density, temperature and interfacial tension had much less influence on droplet terminal velocity. Flow patterns, which were neglected in the Turner et al. model, were taken into account by Coleman for predicting liquid loading in gas wells, indicating that flow patterns in wellbore might affect liquid loading to some

extent. In addition, Coleman also argued that the Tuner et al. model cannot be used when slug flow prevails in wellbore.

The Turner et al. (1969) model was further improved by Guo et al. (2005) using kinetic energy theory. In this model, the minimum kinetic energy theory and the relationship between kinetic energy and terminal velocity were introduced. Guo et al. concluded that the minimum gas velocity to lift liquid droplets corresponded to the minimum kinetic energy of gas flow required to lift liquid droplets,

$$E_k = \frac{\rho_G v_G^2}{2 g_c} \tag{2.2}$$

Where E_k is gas specific kinetic energy, lb_f-ft/ft^3, v_G is gas velocity, ft/s and g_c is unit conversion factor, lb_m-ft/lb_f-s^2.

By case study, Guo et al. (2005) further argued that the prediction results by Turner et al. model still underestimated liquid loading onset even after 20% upward adjustment. It was shown that Guo et al. model gave better predictions than Turner et al. model.

Girija (2007) conducted experimental investigation to observe liquid loading behavior in tubing-casing annulus. Girija concluded that the terminal velocity in tubing-casing annulus from his experiment is 20% to 50% lower than the terminal velocity predicted by Turner et al. model. Two flow patterns, annular flow and transitional annular flow, were observed in experiments.

Zhou (2009) proposed an improved model based on Turner et al. (1969) model with consideration of liquid holdup in gas wells. A model called liquid-droplet concentration model was introduced, considering that the terminal velocity was affected significantly by liquid droplet concentration. If liquid droplet concentration is above the

threshold value (β), the calculation of liquid holdup in gas wells should be included in liquid droplet concentration model. Below this threshold, Turner et al. model is opted. The value of β is a constant number around 0.6 estimated from the Turner et al. model.

For $H_L \leq \beta$

$$v_{t-zhou} = v_{t-turner} = 1.593 \frac{[\sigma_L(\rho_L - \rho_G)]^{1/4}}{\rho_g^{1/2}} \quad 2.3$$

For $H_L > \beta$

$$v_{t-zhou} = v_{v-turner} + \ln \frac{H_L}{\beta} + \alpha \quad 2.4$$

Where $v_{t\text{-}zhou}$ is the terminal velocity of Zhou et al. model, ft/s, $v_{t\text{-}turner}$ is the terminal velocity of Turner et al. model, ft/s and H_L is liquid holdup.

Veeken (2009) observed that the predicted gas flow rates by Turner et al. model were 40% below field data. A modified Turner et al. model would give good matches with the field data. Furthermore, Veeken concluded that, liquid loading in gas wells occurs if bottom-hole pressure reached the minimum value on the outflow curve.

Multiphase flow model was used to describe and analyze liquid loading phenomenon in Veeken's study. Model results agreed with experimental observations. The dominant mechanism of liquid loading onset was found to be liquid film reversal rather than liquid droplet falling.

1.1.2 Mechanistic Model

Mechanistic multiphase flow models can also be used in liquid loading predictions. In mechanistic models, the onset of liquid loading in gas wells can be

predicted by the overall liquid accumulation including liquid film and droplets. This liquid accumulation is manifested by the liquid film velocity reversal and transition from friction dominance to gravity dominance reflected by the minimum bottom pressure.

van't Westende (2008) conducted experimental study in 2-in ID flow loop to observe liquid droplet size and velocity. The results of liquid droplet size measurement revealed that the droplet size was smaller than that used in Turner et al. (1969) model. The flow patterns observed in van't Westende experiments were annular flow and churn-annular flow. He concluded that film instability might have resulted in liquid loading onset since no falling liquid droplets were observed in the experiment.

A more recent experimental study on liquid loading onset in vertical and deviated wells was conducted by Yuan (2011) in a 3-in ID flow loop. Experimental results showed that, in vertical wells, liquid loading onset was due to liquid film reversal and flow pattern transition from fully-developed annular flow to partially-developed annular flow. In deviated wells, liquid loading occurred since liquid film flowed downward continuously at the lower side of the tubing. At the minimum pressure gradient, flow regime changed from fully-developed annular flow to partially-developed annular flow, which triggered liquid loading.

Although liquid loading in vertical wells is slightly different from that in deviated wells, liquid film reversal is consistently verified as the main reason for liquid loading. Yuan proposed the criterion of minimum pressure gradient for onset of liquid loading and pressure gradient fluctuation at the same time.

Moreover, Yuan (2011) also found that liquid film oscillated in unloading wells when it began to reverse. The upward interfacial waves intercepted liquid film from

flowing downward continuously and led to liquid film periodical downward flowing under the waviness.

Gunner (2012) studied liquid loading in vertical and deviated gas wells after Yuan's (2011) research. With similar experimental results, Gunner also found that the liquid loading onset associated with the minimum pressure gradient and pressure gradient fluctuations happened at the same time.

Gunner compared calculated results using Barnea (1987) model with experimental data. It was found that the critical gas velocity was the gas velocity at the minimum pressure gradient from Barnea model, which corresponded to the liquid film reversal.

Gunner concluded that well deviation was an important factor affecting gas terminal velocity. When the well is close to vertical, the gas terminal velocity is high. She pointed out that superficial gas velocity was equal to the critical gas velocity which could be used to predict onset of liquid loading in gas wells.

1.1.3 Zhang et al. Unified Model

Zhang et al. (2003) unified model predicts multiphase flow hydrodynamics and flow patterns all from basic equations via slug dynamics, while other mechanistic models start with equilibrium stratified flow. The Zhang et al. unified model can be applied to wells with all inclination angles. Liquid film velocity is one of the main parameters which characterize slug and annular flows. It also plays an important role in liquid loading prediction. Thus, liquid film velocity calculated from Zhang et al. unified model will be analyzed.

Zhang et al. unified model was validated with experimental results covering different pipe diameters, fluid properties, inclination angles, gas and liquid flow rates, and flow patterns. It gives good predictions of flow patterns, liquid holdup, film thicknesses and pressure gradients in wellbores and pipelines with different inclination angles.

1.2 Plunger Lift Modeling

Foss and Gaul (1965) reported over 100 wells that used plunger lift in the Ventura Avenue Field operated by Shell Company. A simplified static model of plunger lift based on those field cases was proposed. By analyzing force balance on the plunger, a set of plunger lift performance curves were generated, which are still widely used as references to compare with new models proposed by later researchers.

In the static model, the plunger rising and falling velocities were assumed as constants. The rise velocities are 1000 ft/min and 172 ft/min through gas and liquid, respectively. The falling velocity is 2000 ft/min through gas. Gas column weight, plunger friction and gas friction are neglected. Foss and Gaul also presented that the cycle frequency of the plunger was related to the productivity index of the well, tubing back pressure, available gas energy and plunger travel time. The maximum cycle was calculated based on well length and load size at the intersection of the proper depth.

Lea (1982) proposed a dynamic model of plunger lift, as opposed to the Foss and Gaul (1965) static model. The force balance equation on plunger was used to develop the dynamic model. Lea obtained plunger positions, velocity, acceleration and casing pressure by solving the force balance equation numerically. Gas and liquid frictions were

taken into account. A simplified liquid loading expression as function of time and gas flow rate was used in the model. However, gas leakage and liquid fallback from plunger were neglected. Similar cycle frequency equation as presented by Foss and Gaul was used in the dynamic model. The calculated results were compared with Foss and Gaul model predictions. It was found that, for Foss and Gaul model with constant plunger rising and falling velocities, 16% more gas is needed to lift plunger than that for Lea model.

Mower et al. (1985) conducted plunger lift tests on pressure, velocity, gas and liquid volumetric flow rates for 13 different commercial plungers rising and falling in gas wells. Experimental results also included gas leakage and liquid fallback. For different plungers, the optimum plunger rising velocities varied. However, for most plungers, the optimum plunger rising velocity was around 1000 ft/min. From the testing results, it was concluded that gas slippage was a significant factor affecting plunger lift efficiency. In addition, an interesting observation from experiments was that gas slippage decreased as plunger velocity increased, which also led to liquid fallback increasing. Mower et al. also presented a model accounting for gas slip and liquid fallback to match test data.

Marcano and Chacín (1994) proposed a new mechanistic model for predicting conventional plunger lift process. The liquid fallback during plunger rise was treated as a linear function of average velocity. A Fortran-based simulator was programed to calculate liquid fallback losses and estimate the optimum cycle time. However, due to lack of sufficient field data, this model was validated partially. Further validation is needed to show its feasibility.

Charcin (1990) conducted mathematical modeling and optimization of intermittent gas-plunger lift operations (Figure 4). By combining plunger lift process and reservoir inflow performance, a new plunger lift model was developed, which can be used to simulate gas-plunger lift operation. The model assumed constant plunger rising and falling velocities. However, in the model validation, it was found that plunger falling velocity seemed to be a major factor in determining overall performance of plunger lift. Thus, Charcin pointed out that plunger velocity should be emphasized during modeling the plunger lift process. Meanwhile, the formation water-oil ratio and gas-oil ratio should also be considered in developing plunger lift model.

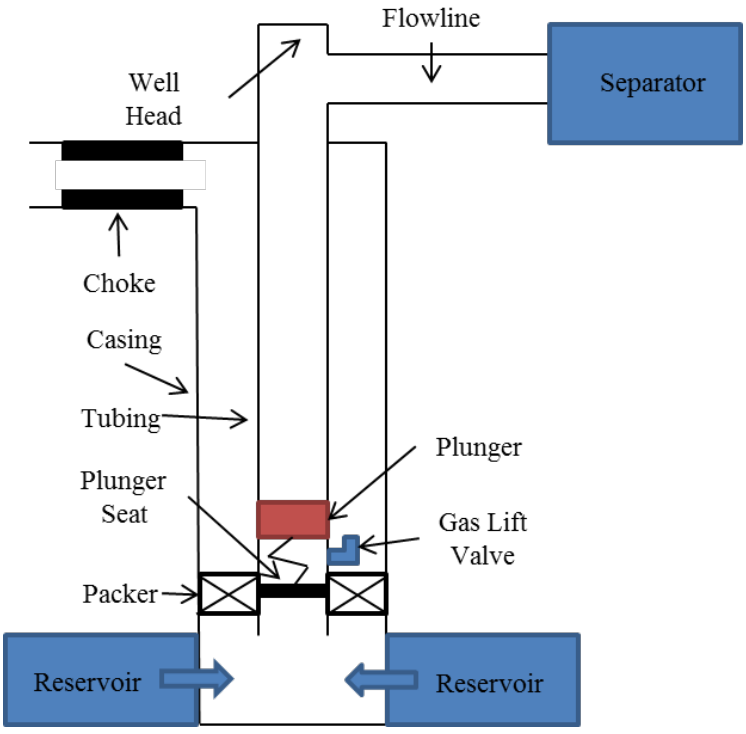

Figure 4: Intermittent Plunger Lift

Gasbarri and Wiggins (2001) proposed a plunger lift model that comprises of four parts: upstroke, blowdown, build-up and reservoir performance. Upstroke covers the

dynamics of plunger rising and liquid slug movement by the plunger lift. The gas section changes above the slug and below the plunger (Figure 5) are also included. Blowdown is slug production to the separator from tubing string. It also accounts for gas production after the plunger reaches the surface. Build-up covers the liquid accumulation in gas wells and system pressure or bottomhole pressure increase. Reservoir performance is fluid flow from reservoir to wellbore during the entire process of plunger lift operation. Fundamental conservation equations were used to derive the dynamic model. Gasbarri and Wiggins model avoided some assumptions in previous plunger lift models proposed by other researchers. Transient behavior of gas above the liquid slug was considered in the upstroke step when the tubing valve was open. Gasbarri and Wiggins model also combined the dynamics of plunger lift with reservoir performance.

A plunger lift simulator based on Fortran was developed by Gasbarri and Wiggins (2001), and was validated with Lea (1982) well examples and field data from Baruzzi and Alhanati (1995). The comparison of model predictions with field data was good, although liquid fallback through the gap between plunger and tubing (as plunger moved upward) was not considered in the model. It should be noticed that, plunger falling velocities of Gasbarri and Wiggins (2001) model after wells shut-in were assumed constant, 1000 ft/min in gas and 175 ft/min in liquid.

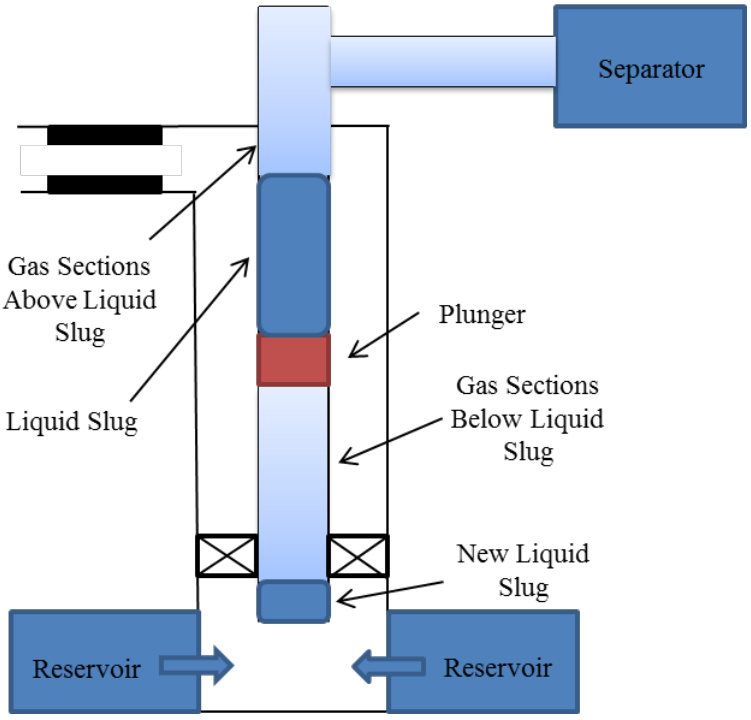

Figure 5: Gas Sections below and above Liquid Slug

CHAPTER 2

MODEL DEVELOPMENT

In this chapter, liquid loading onset in gas wells is analyzed based on Zhang et al. (2003) unified model. The plunger lift working process is modeled with equations presented in previous studies and new improvements are added in the closure relationships.

2.1 Liquid Loading Onset Prediction

Multiphase flow mechanistic models can predict pressure gradients, liquid holdup, and film velocity among many other parameters for flow characterization. These parameters are also directly or indirectly related to liquid loading. Experimental studies on multiphase pipe flow have also been performed to validate the mechanistic models.

The Veeken (2009), van't Westende (2008), Yuan (2011) and Gunner (2012) experimental studies found that liquid loading onset was related to liquid film reversal and minimum pressure gradient. Proposals have been made to use these two parameters to predict liquid loading onset in gas wells.

The Zhang et al. (2003) unified model is a new generation mechanistic model for multiphase flow in pipe with any inclination angles. The multiphase hydrodynamics and flow pattern are all predicted from the basic momentum equations. The liquid film velocity and pressure gradient predicted by the unified model corresponding to the liquid

loading onset observed in experiment are analyzed. A criterion is proposed for the prediction of liquid loading onset.

2.1.1 Pressure Gradient Method

Veeken (2009) concluded that liquid loading in gas wells occurs when the bottom pressure (or pressure gradient) on outflow performance curve reaches the minimum value. Yuan (2011) and Gunner (2012) confirmed Veeken's observation of liquid loading onset through analyzing their pressure gradient measurements (as shown in Figure 6).

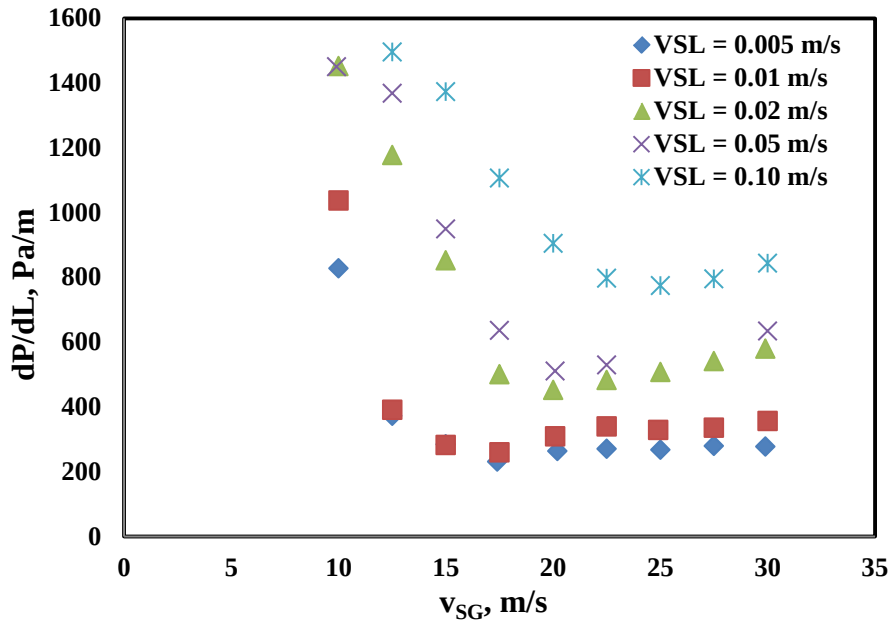

Figure 6: Pressure Gradient vs. Superficial Gas Velocity in Vertical Pipe (Yuan 2011)

Figure 6 shows pressure gradients measured by Yuan (2011) versus superficial gas velocity at different superficial liquid velocities (v_{SL} = 0.005, 0.01, 0.02, 0.05 and 0.10 m/s.) in vertical pipe. As superficial gas velocity decreases gradually, flow pattern in

the pipe changes from fully developed annular flow to partially developed annular flow. When pressure gradient reaches the minimum value, liquid loading occurs. It appears that liquid loading onset can be predicted by the minimum pressure gradient locality and flow pattern transition.

Flow patterns in gas wells are mostly annular flow and intermittent flow. Different multiphase flow models may define flow pattern transition differently. The transition between two adjacent flow patterns is normally not a distinct boundary, but a zone. Thus, it is hard to predict liquid loading onset using the flow pattern transition criterion. However, pressure gradients are standard outputs of mechanistic models for multiphase pipe flow. At high gas flow rate (velocity), liquid holdup (loading) is low. As a result, gravitational pressure gradient is low and frictional pressure gradient is dominant. At low gas flow rate (velocity), liquid loading occurs and liquid holdup is high. Gravitational pressure gradient becomes dominant in vertical or near-vertical wells. Therefore, the minimum total pressure gradient corresponds to the transition from friction dominant flow to gravity dominant flow. The increase of liquid loading causes this transition.

2.1.2 Liquid Film Velocity Method

Turner et al. (1969) examined the film reversal approach for liquid loading prediction but pointed out that it was inaccurate compared with the liquid droplet falling approach. Thereafter, several researchers developed new liquid loading prediction models and conducted experiments on liquid loading in pipes with varying inclination angles, to validate the proposed models. Some recent researchers realized that liquid film reversal

turned out to be more important than liquid droplet falling for liquid loading prediction. Veeken (2009) pointed out that the Turner et al. droplet model was too conservative to accurately estimate the droplet terminal velocity compared with data. He also argued that liquid film reversal was the main mechanism of liquid loading onset.

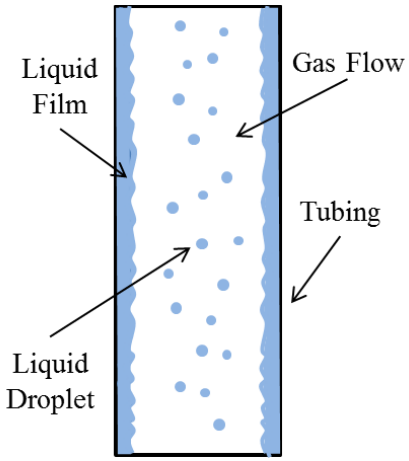

Figure 7: Liquid and Gas Distribution in Wells

Experimental observations show that liquid loading occurs under slug flow or intermittent flow, which leads to higher liquid holdup due to slippage between gas and liquid. If gas flow rate is high enough, a large amount of liquid can be entrained in the gas core as dispersed droplets. On the pipe wall a thin liquid film will form (as shown in Figure 7).

The liquid film reversal theory can be explained with the force balance on the liquid film. In gas-liquid annular flow, gas flows at the center with entrained liquid droplets. A thin annular liquid film around the pipe wall also flows upward but with a much lower velocity. The shear force on the liquid film by the gas core exceeds the

gravity of the liquid film. The difference is balanced by the friction between the liquid film and pipe wall.

The reservoir will deplete with continuous production. As a result, bottomhole pressure will decrease causing flow rate decrease. When gas velocity becomes lower, its shear force on the interface will be less. When shear force approaches the gravity of the liquid film, the film velocity will slow down to zero. After that, liquid film velocity will become negative and reversal liquid film flow will occur. Liquid loading starts due to the reversal flow of liquid film. Using mechanistic multiphase flow models, it is possible to predict liquid loading onset with the predicted film velocity (liquid film reversal theory). In Zhang et al. unified model, liquid film velocity can be obtained from the momentum conservation equations.

2.2 Plunger Lift Modeling

Plunger lift model can be divided into six components namely, plunger upstroke, gas blowout, plunger fall down, pressure buildup, gas flows above and below plunger and reservoir performance.

Above and below plunger, gas flows with plunger moving in the tubing. Reservoir performance is a component included in all stages of plunger lift processes. In energy buildup stage, reservoir performance contributes to restoring energy below the plunger.

Basic mass and momentum conservation equations are used to derive the plunger lift simulation model. Several conservation momentum equations are cited from Gasbarri and Wiggins (2001) study and applied to plunger upstrokes and gas section procedures.

2.2.1 Plunger Upstroke

Plunger upstroke is a dynamic process during which the plunger moves upward from tubing bottom. When the plunger travels from bottom hole to the wellhead, it involves three parts: gas section above the liquid slug, plunger and slug movement, and gas section below the plunger (as shown in Figure 8).

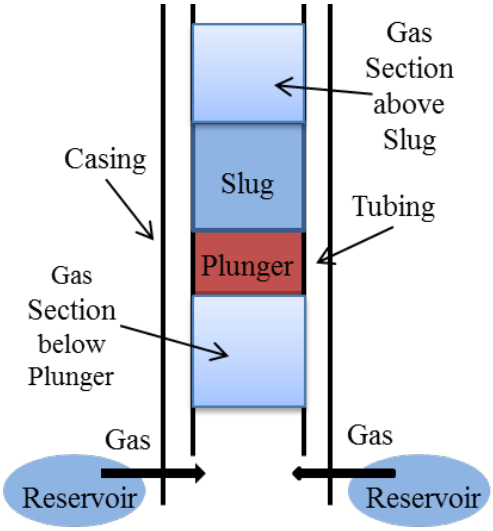

Figure 8: Plunger, Liquid Slug, and Gas Sections below and above Plunger

The plunger movement is analyzed with boundary conditions including pressures at slug top and plunger bottom. Slug top pressure can be solved through the gas section above the slug when the plunger moves up. Plunger bottom pressure can be solved through the gas section below the plunger from the connection with casing-tubing annulus.

For liquid slug and plunger moving upward in tubing, the momentum equations applied to single phase liquid with constant density are based on Lea (1982) model. On the control volume in the moving system, the volume is assumed constant during the

plunger and slug traveling in the tubing. The acceleration of the slug can be obtained from the momentum equations. Figure 9 shows the forces acting on the slug and plunger in tubing.

In addition, Gasbarri and Wiggins (2001) developed an upstroke model for plunger lift. Using momentum balance equations to describe plunger movement in the tubing, this method is widely accepted by researchers to model plunger lift process. The Gasbarri and Wiggins upstroke model is also adopted in this study to describe plunger upward movement and gas behavior accompanying the plunger movement.

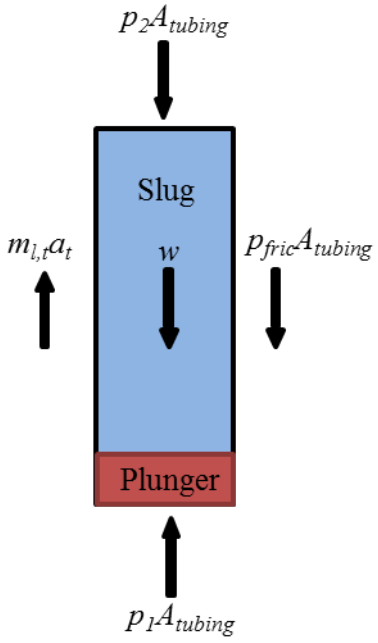

Figure 9: Force Balance of Plunger Upstroke (Plunger and Slug in Tubing)

When the plunger moves upward and the slug is far from wellhead, the momentum equation based on the force balance on the control volume is written below. It

is applied to vertical direction. The slug acceleration can be solved from this momentum equation.

$$m_{l,t}a_t = (p_1 - p_2)A_{tubing} - w - f_l \rho_l A_{tubing} \frac{L_t}{2d_t} v_{l,t}^2 \quad (3.1)$$

$m_{l,t}$ is mass of liquid slug and plunger in the tubing, kg. ρ_l is liquid slug density, kg/m^3. a_t is acceleration of liquid slug and plunger in the tubing, m/s^2. p_1 is pressure below plunger, Pa. p_2 is pressure above plunger, Pa. A_{tubing} is tubing cross sectional area, m^2. w is total weight of liquid slug and plunger, kg. f_l is tubing friction factor. L_t is slug length in the tubing, m. d_t is tubing diameter, m. $v_{l,t}$ is slug velocity in the tubing, m/s.

When slug reaches the wellhead and begins to flow into pipeline on surface, the liquid mass and length of the vertical control volume will decrease. Figure 10 shows the forces acting on slug and plunger control volume after the slug reaches the surface pipeline. The momentum equation below based on this force balance can be used to solve the slug acceleration.

$$m_{l,t}a_t = (p_1 - p_2)A_{tubing} - w - f_l \rho_l A_{tubing} \frac{L_t}{2d_t} v_{l,t}^2 - \sum_{CS} v_{l,t} \rho_l A_{tubing} u_{l,t} \quad (3.2)$$

$u_{l,t}$ is slug velocity in the tubing, m/s.

When liquid starts to flow in the surface pipeline, the liquid slug length increases. The momentum equation for slug in the surface pipeline can be expressed below based on the force balance on the control volume shown in Figure 11.

$$m_{l,L}a_L = (p_2 - p_3)A_L - f_L \rho_l A_L \frac{L_L}{2d_L} v_{l,L}^2 - \sum_{CS} v_{l,L} \rho_l A_L u_{l,L} \quad (3.3)$$

$m_{l,L}$ is mass of liquid slug in the surface pipeline, kg. a_L is acceleration of liquid slug in the surface pipeline, m/s^2. p_3 is pressure at the front of slug in the surface pipeline, Pa. L_L

is slug length in the surface pipeline, m. $v_{l,L}$ is slug velocity in the surface pipeline, m/s. $u_{l,L}$ is slug velocity in the surface pipeline. A_L is surface pipeline cross sectional area, m^2. d_L is surface pipeline diameter, m. f_L is friction factor in the surface pipeline.

The slug acceleration can be obtained through combing Equation 3.1 and Equation 3.2,

$$a_t = \frac{p_1 - p_3 - f_l \rho_l v_{l,t}^2 \frac{L_t}{2d_t} - f_L \rho_l v_{l,L}^2 \frac{L_L}{2d_L}\left(\frac{A_t}{A_L}\right)^2 - \frac{\kappa \rho_l v_{l,t}^2}{2g} - \frac{w}{A_{tubing}}}{\frac{m_{l,t}}{A_{tubing}} + \frac{m_{l,L} A_{tubing}}{A_L^2}} \quad 3.4$$

κ is the empirical friction factor of flow through the tee section.

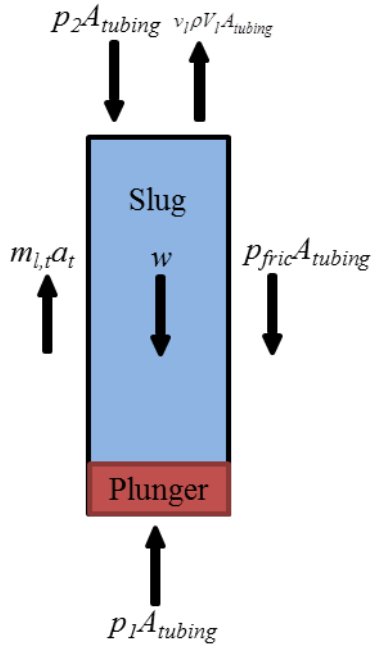

Figure 10: Force Balance of Plunger Upstroke (Plunger Reaching to Wellhead)

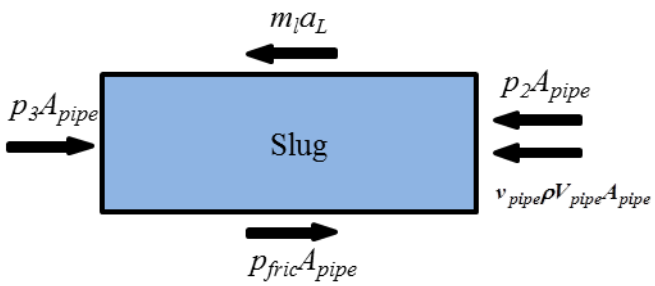

Figure 11: Force Balance of Plunger Upstroke (Slug Flowing in Surface Pipeline)

2.2.2 Gas Blowout

The gas blowout component describes gas well production with wellhead valve opened after plunger reaches wellhead for a certain time period. In gas blowout phase, hydrocarbon fluid is produced from reservoir. Meanwhile, liquid starts to load up at the bottom of gas well. The gas blowout phase ends when gas cannot be produced at a satisfactory rate because of liquid loading in the gas well. Engineers have to decide the gas blowout time. For this process, Gasbarri and Wiggins (2001) developed a model based on momentum equations. In this study, the Gasbarri and Wiggins model for gas blowout components is incorporated in the new plunger lift model.

The same assumptions as the plunger upstroke component are made for the gas blowout component. Liquid is produced with gas from reservoir and the flow pattern at the bottom is assumed to be slug flow. Force balance analysis on the liquid slug is made similarly as that for the plunger upstroke component. The liquid slug is assumed to completely fill the tubing.

$$m_{l,L} a_L = (p_2 - p_3) A_L - f_L \rho_L A_L \frac{L_L}{2 d_L} v_{l,L}^2 \quad 3.5$$

2.2.3 Plunger Downstroke

Plunger downstoke component is the phase during which the plunger moves downward from wellhead to the well bottom after gas blowout phase. The plunger falls down once gas blowout is stopped. A proper time for the plunger to fall down to the well bottom also needs to be specified by engineers.

Generally, constant plunger falling velocities were used in most previous plunger lift models. Gasbarri and Wiggins (2001) model assumed the plunger falling velocity to be 1000 ft/min in gas phase and 175 ft/min in liquid phase. However, they pointed out that the plunger lift velocities should be modified for different well conditions. In this study, plunger falling velocity is calculated from plunger acceleration, which is dependent on well flow conditions.

Due to liquid accumulation at the bottom of gas wells, the plunger downstroke movement includes two parts. One is the plunger traveling in gas phase and the other is the plunger traveling in liquid phase. Therefore, plunger accelerations in gas and liquid phases must be formulated separately.

Figure 12 shows the schematic of plunger downstroke movement. The forces acting on the plunger are used to obtain plunger falling acceleration. As shown in Figure 12, these forces include gravity force and drag force. Thus, if plunger falls at a constant velocity the plunger gravity should equal to drag force.

Figure 12: Force Balance of Plunger Downstroke

As discussed above, the acceleration of the plunger moving downward in the gas phase is a function of plunger gravity, drag coefficient, gas density, plunger velocity and plunger diameter. In order to calculate the plunger falling velocity accurately, more detailed plunger geometrical information is needed in the new model. In the plunger lift simulator, specific drag coefficients corresponding to different plunger geometries are incorporated, from which a proper value of drag coefficient can be selected automatically when calculating plunger falling velocity. Meanwhile, gas density is affected by local well temperature and pressure. The calculation methods and equations can be found in Appendix B. Plunger acceleration and falling velocity can be calculated by:

$$a_{plunger} = \frac{m_{plunger} g - \frac{0.5 C_d \rho_G \pi}{4} D_{plunger} v_{plunger}^2}{m_{plunger}} \quad 3.6$$

$$v_{plunger} = \sqrt{\frac{m_{plunger} g}{0.5 C_d \rho_G \frac{\pi}{4} D_{plunger}}} \quad 3.7$$

$a_{plunger}$ is plunger acceleration, m/s^2. $m_{plunger}$ is mass of the plunger, kg. $D_{plunger}$ is plunger diameter, m. $v_{plunger}$ is plunger falling velocity, m/s.

Plunger velocity is also affected by plunger mass, gravity, liquid density, drag coefficient, and plunger diameter.

$$a_{plunger} = \frac{m_{plunger} g - \frac{0.5 C_d \rho_L \pi}{4} D_{plunger} v_{plunger}^2}{m_{plunger}} \quad 3.8$$

$$v_{plunger} = \sqrt{\frac{m_{plunger} g}{0.5 C_d \rho_L \frac{\pi}{4} D_{plunger}}} \quad 3.9$$

2.2.4 Buildup and Reservoir Performance

Energy buildup component and reservoir performance component are combined together in the model. A seat at the bottom of the well is used to host the plunger, which enables an energy buildup for the plunger before starting the next circle. The energy buildup component describes the accumulation of reservoir energy under the plunger seat at well bottom when the plunger is locked on the seat. When the reservoir energy (pressure) reaches a certain level, the seat locker will open and plunger will start to travel upward again.

Reservoir performance component describes reservoir behavior or inflow performance of gas wells (IPR). It works continuously during the plunger lift cycle (Figure 13).

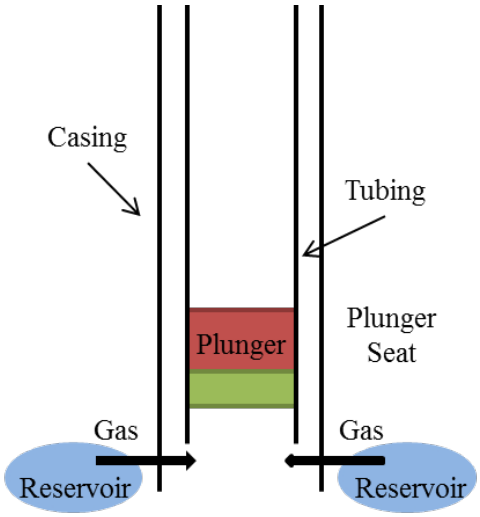

Figure 13: Reservoir Performance

In the new model, both steady and unsteady state inflow performance relationships of gas wells are considered. During plunger lift, fluid flow decreases with liquid loading and increases after the liquid slug is lifted. Therefore, the inflow from reservoir to bottomhole is unsteady. The productivity equations (J-factor function) are used to describe reservoir performance in the new model while Gasbarri and Wiggins used Rawlins and Schellhardlt's (1935) empirical functions (backpressure method) in their model. For steady state flow, gas production flow rate is the function of gas viscosity, well temperature, well pressure, reservoir permeability, gas compressibility, drainage radius and well radius, standard gas density, reservoir pressure and reservoir thickness.

If value under the square root of Eq. (3.10.2) is larger than zero,

$$\boldsymbol{Q_g = A - \frac{B}{C}} \qquad 3.10$$

$$A = \frac{\frac{\mu Z}{\pi k h}\left(\frac{P_{SC}T}{T_{SC}Z_{SC}}\right)\log\left(\frac{R_e}{R_w}\right)}{2\rho_{g,SC}\left(\frac{Z}{2\pi^2 h^2}\right)\left(\frac{P_{SC}T}{T_{SC}Z_{SC}}\right)\left(\frac{1}{R_w}-\frac{1}{R_e}\right)} \qquad 3.10.1$$

$$B = \sqrt{\frac{\frac{\mu Z}{\pi k h}\left(\frac{P_{SC}T}{T_{SC}Z_{SC}}\right)\log\left(\frac{R_e}{R_w}\right)}{2\rho_{g,SC}\left(\frac{Z}{2\pi^2 h^2}\right)\left(\frac{P_{SC}T}{T_{SC}Z_{SC}}\right)\left(\frac{1}{R_w}-\frac{1}{R_e}\right)}} \qquad 3.10.2$$

$$C = 2\rho_{g,SC}\left(\frac{Z}{2\pi^2 h^2}\right)\left(\frac{P_{SC}T}{T_{SC}Z_{SC}}\right)\left(\frac{1}{R_w}-\frac{1}{R_e}\right) \qquad 3.10.3$$

μ is gas viscosity, cp. Z is gas compressibility. k is gas permeability, md. h is thickness of pay zone, m. P_{SC} is pressure at standard condition, Pa. T is local temperature, K. T_{SC} is temperature at the standard condition, K. Z_{SC} is gas compressibility at standard condition. R_e is radius of drainage area, m. R_w is radius of the wellbore, m. $\rho_{g,SC}$ is gas density at standard condition, kg/m^3.

If value under the square root of Eq. (3.10.2) is less than zero,

$$Q_g = \frac{\left(P_e^2 - P_w^2\right)}{\frac{\mu Z}{\pi k h}\left(\frac{P_{SC}T}{T_{SC}Z_{SC}}\right)\log\left(\frac{R_e}{R_w}\right)} \qquad 3.12$$

P_e is reservoir pressure, Pa. P_w is pressure at the bottomhole, Pa.

For unsteady state flow, gas production rate is function of reservoir pressure, well pressure, well temperature, gas compressibility, reservoir permeability, pay zone thickness, well radius and oil viscosity.

$$Q_g = \frac{\left(P_R^2 - P_w^2\right)}{\left(\frac{\mu}{2\pi h k}\right)\left(\frac{PZT}{T_{sc}Z_{sc}}\right)\log\left(\frac{2.25kt}{\mu C_t R_w^2}\right)} \qquad 3.13$$

where is C_t is the total compressibility, psi^{-1}.

CHAPTER 3

PLUNGER LIFT SIMULATOR

A computer program is written in Visual Basic language with Visual Studio 2010 to implement the new plunger lift model described in the previous chapter. The simulator consists of three main parts. The first part is Data Input. The second is Simulation and the third Data Analysis. Each part is accommodated with a Graphic User Interface (GUI) which contains sub-interfaces.

3.1 Data Input Interface

Data Input interface has five sub-interfaces including Well Geometry, Surface Parameters, Fluid Properties, Reservoir Parameters and Special Parameters. All required information for simulation is provided by these five sub-interfaces.

The sub-interface Well Geometry is the window for inputting parameters which describe the well profile and plunger properties. The well profile includes well depth, tubing inner diameter, tubing outer diameter, casing inner diameter and casing outer diameter. Plunger properties include plunger outer diameter and plunger mass. The drag coefficients of different plungers are defined in the program. The unit of length is in meter and the unit of mass in kilogram. There are two plunger type options namely casing-tubing type and tubing type. Figure 14 shows the Well Geometry interface.

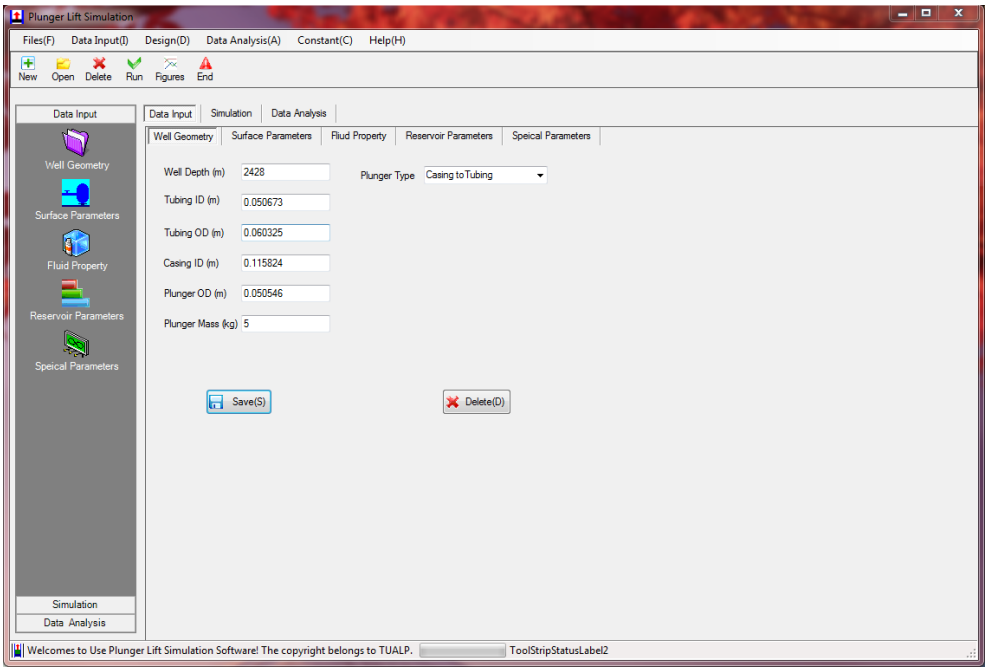

Figure 14: Well Geometry Interface

The sub-interface Surface Parameters is the window for inputting parameters defining surface pipeline and separator. This information is needed to calculate plunger traveling velocity, hydrocarbon production rate and gas sections in tubing and surface pipeline. The input parameters include surface pipe length, surface pipe inner diameter and surface pressure (separator pressure). The unit of pressure is in MPa. Figure 15 is a snap shoot of the Surface Parameters interface.

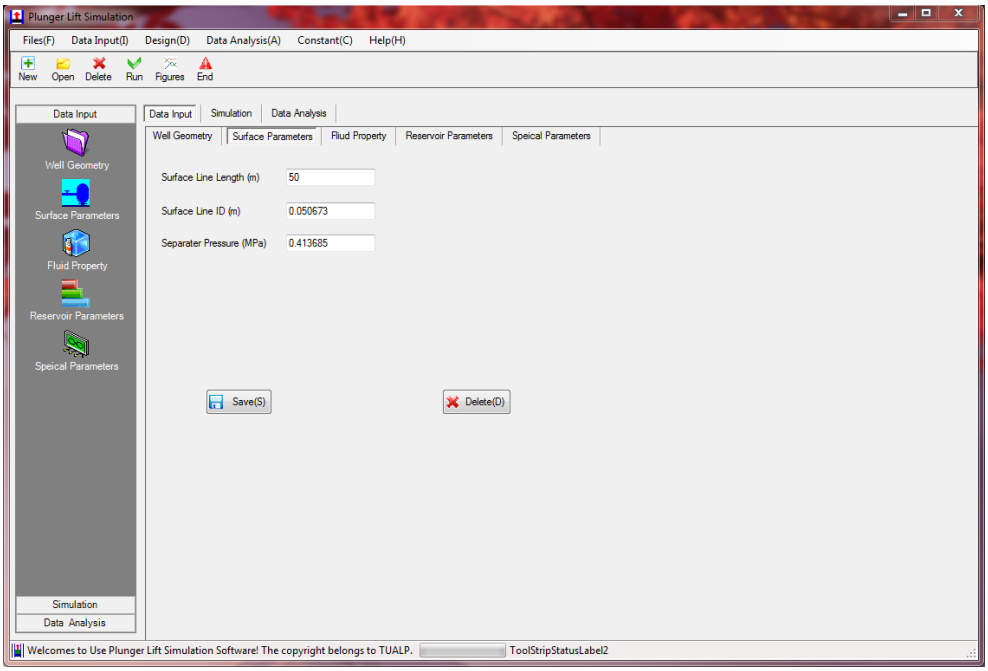

Figure 15: Surface Parameters Interface

The sub-interface Fluid Properties is for inputting the liquid and gas properties. Liquid phase can be oil, condensate, water, or a mixture of oil and water. The inputs include liquid density, gas specific gravity and initial liquid length (slug length). The unit of density is in kilogram per cubic meter. Figure 16 shows the Fluid Properties interface.

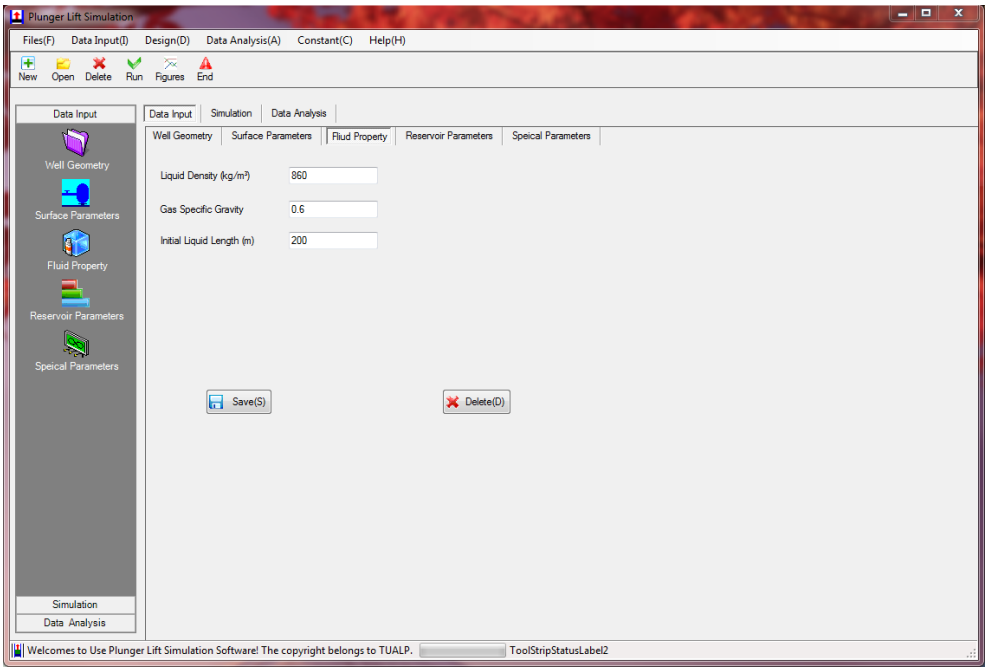

Figure 16: Fluid Properties Interface

The sub-interface Reservoir Parameters is for inputting reservoir information, which is used to characterize the inflow performance relationship (IPR). IPR together with the bottomhole flowing pressure provides hydrocarbon production rate. Bottomhole flowing pressure is calculated using the pressure gradient along the wellbore. The inputs include reservoir pressure, gas permeability, reservoir thickness, drainage radius, geothermal gradient, surface temperature, well diameter, liquid gas ratio, coefficient *C* and exponent *n*. The unit of permeability is in milli-Darcy. The unit of surface temperature is in Kelvin, and the geothermal gradient unit is in Kelvin per meter. Figure 17 shows Reservoir Parameters interface.

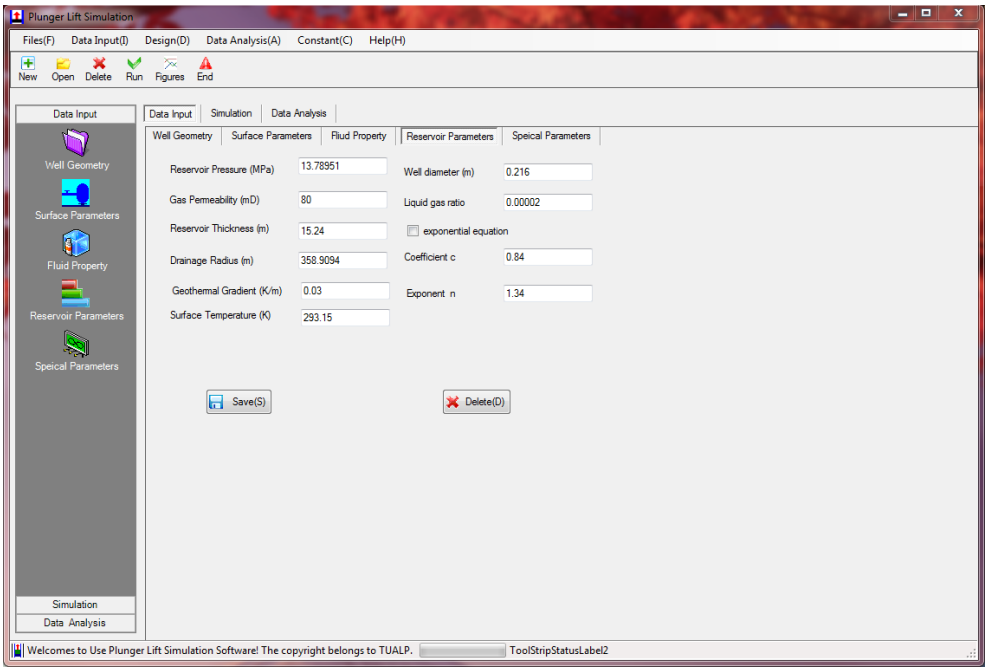

Figure 17: Reservoir Parameters Interface

The sub-interface Special Parameters is for inputting additional parameters. In the present model, absolute roughness is required for pipeline, tubing and casing wall surfaces. It is used to calculate friction factor, which is further used to calculate the casing and tubing frictional pressure gradients. Figure 18 shows the Special Parameters interface.

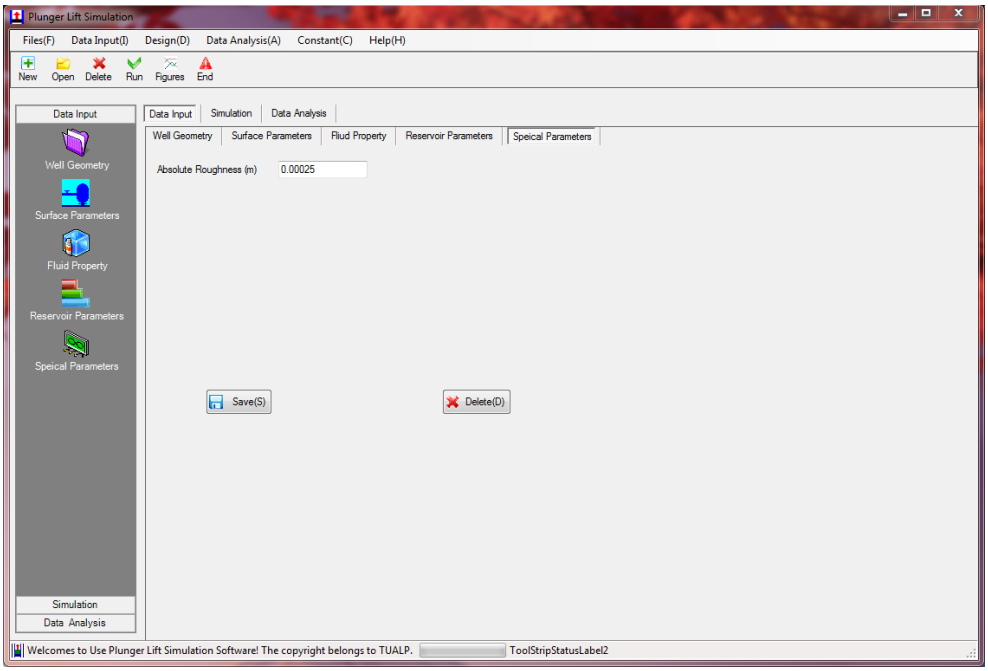

Figure 18: Special Parameters Interface

3.2 Simulation Interface

As shown in Figure 19, Simulation Interface offers two options. The first four command buttons are individually for Up Stroke, Blowout, Down Stroke, and Build Up. Each corresponds to a plunger lift working procedure, as discussed in the Model Development chapter. The second option Circulate integrates all plunger lift working stages together as a complete cycle.

In the display window the plunger lift process is animated along with the simulation. There are two dynamic plots and one animation graph. One plot is plunger velocity (m/s) versus time (s). The second plot is plunger acceleration (m/s^2) versus time (s). The animation graph shows plunger and liquid slug movements simultaneously with the displays of the calculated results.

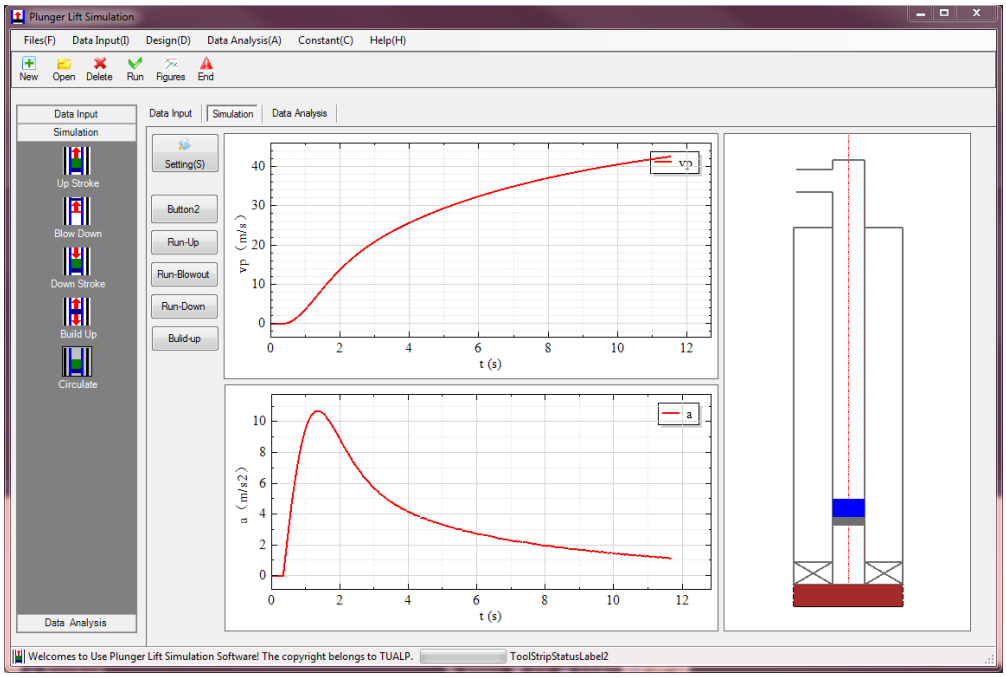

Figure 19: Simulation Interface

3.3 Data Analysis Interface

Data Analysis interface provides all simulation results and plots. With Curves Selection, the simulator offers eleven different curves from the outputs. Users can select any of these plots for analysis or comparison with field data. The simulation outputs include plunger velocity (m/s), plunger acceleration (m/s^2), gas flow rate (m^3/s), bottomhole flowing pressure (Pa), casing pressure (Pa), pressure on the upside of plunger (Pa), surface pipeline outlet pressure (Pa), gas flow rate below the plunger (m^3/s), liquid accumulation in the wellbore (m^3) versus time (s), and plunger velocity (m/s), pressure on the upside of plunger (Pa) versus well depth (m). Figure 20 shows the Data Analysis interface.

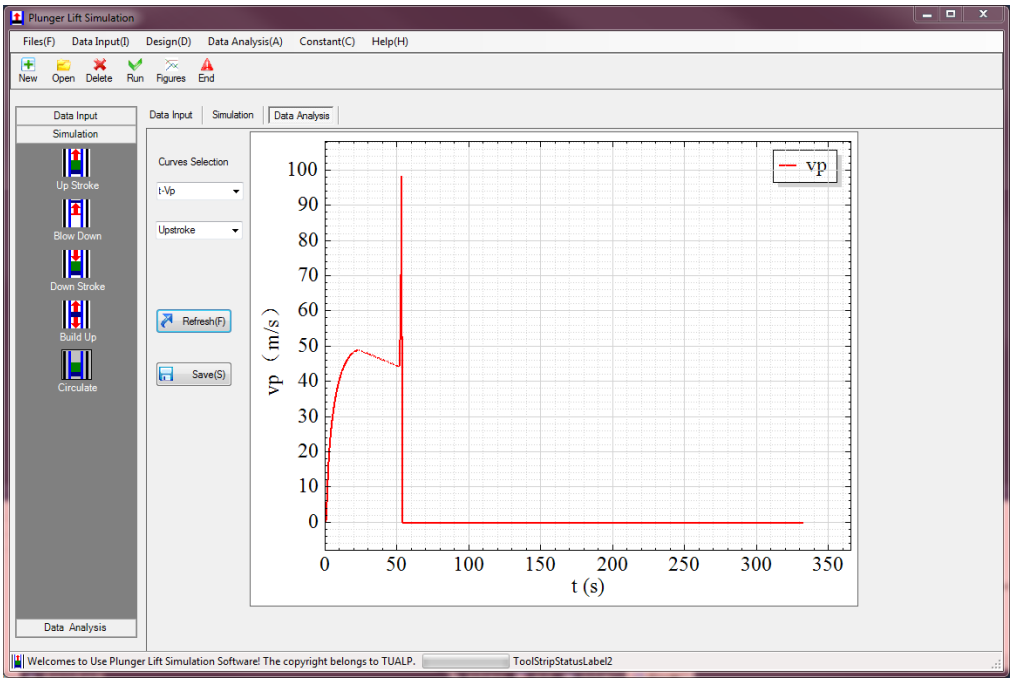

Figure 20: Data Analysis Interface

CHAPTER 4

SIMULATION RESULTS AND DISCUSSIONS

4.1 Liquid Loading Prediction Results

Fluid properties and pipe geometry from Yuan (2011) experimental study are used as inputs for liquid loading onset analyses. Yuan's water-air two phase flow experiments were conducted in a flow loop with pipe inner diameter 3 in. Water density was 998 kg/m^3. Water viscosity was 0.001 Pa·s. Water-air interfacial tension was 0.073 N/m. Outlet pressure was atmospheric pressure. Pipe wall roughness was 0.0028 mm.

Zhang et al. (2003) unified model for multiphase pipe flow is used to analyze liquid loading process in this study. The unified model predictions include pressure gradient and liquid film velocity. The relationship between pressure gradient and liquid loading onset as well as the relationship between liquid film velocity and liquid loading onset are examined in this section.

4.1.1 *Liquid Loading Prediction in Vertical Pipe*

Figure 21 shows pressure gradient versus superficial gas velocity at superficial liquid velocities 0.01, 0.05 and 0.1 m/s. The pressure gradient trends indicate that with superficial gas velocity increase pressure gradient first drops dramatically to (or close to) the minimum value. With further increase of superficial gas velocity, pressure gradient will be flat or slightly increase.

The flow pattern predicted by the Zhang et al. unified model during the sharp drop of pressure gradient is intermittent flow (or slug flow). At the minimum pressure gradient, liquid loading experiences a transitional change based on model predictions and experimental data. The critical gas flow rate is defined as corresponding to the minimum pressure gradient. If gas flow rate is lower than the critical value, liquid loading should occur. Table 1 lists the critical superficial gas velocities and the correspondent minimum pressure gradients at different superficial water velocities in vertical pipe.

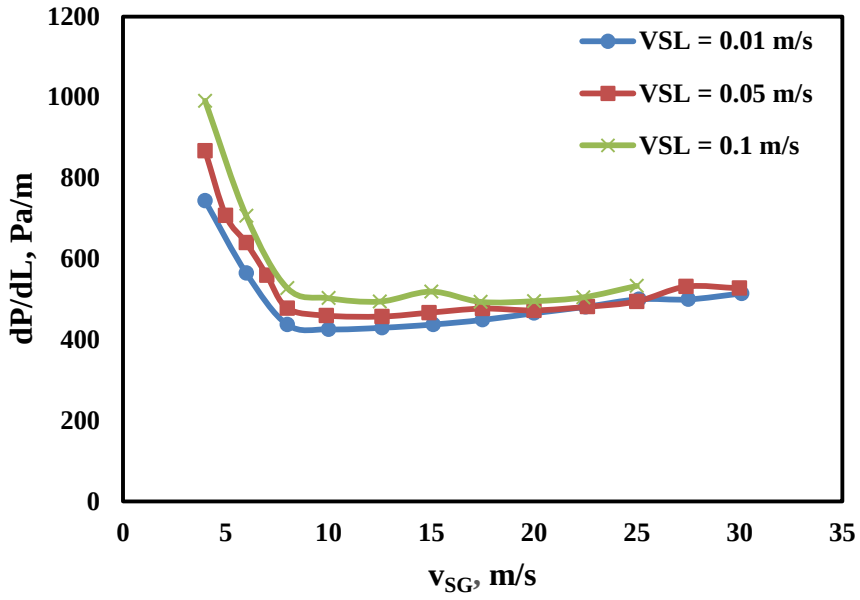

Figure 21: Pressure Gradient vs. Superficial Gas Velocity in Vertical Pipe

Table 1: Critical Gas Superficial Velocities at Different Superficial Water Velocities in Vertical Pipe

v_{SW}, m/s	v_{SGC}, m/s	$(Dp/dL)_M$, Pa/m	θ, °	Loading
0.01	10.0	426.02	90	Yes
0.05	12.6	457.76	90	Yes
0.10	17.4	493.99	90	Yes

Table 2: Liquid Loading Related to Liquid Film Velocity in Vertical Pipe

No.	v_{SG}	v_{SL}	v_F	Loading or Not
	m/s	m/s	m/s	-
1	30.0	0.005	-0.11	No
2	27.5	0.005	-0.20	No
3	25.0	0.006	-0.26	No
4	22.6	0.006	-0.31	No
5	20.0	0.006	-0.35	No
6	17.5	0.006	-0.41	No
7	15.0	0.006	-0.47	Yes
8	12.5	0.005	-0.51	Yes
9	10.1	0.005	-0.57	Yes
10	30.1	0.01	-0.18	No
11	27.5	0.01	-0.22	No
12	25.1	0.01	-0.17	No
13	22.5	0.01	-0.25	No
14	20.0	0.01	-0.32	No
15	17.5	0.01	-0.41	No
16	15.1	0.01	-0.48	Yes
17	12.6	0.01	-0.54	Yes
18	10.0	0.01	-0.60	Yes
19	30.0	0.02	-0.18	No
20	27.5	0.02	-0.24	No
21	25.0	0.02	-0.31	No
22	22.6	0.02	-0.35	No
23	20.0	0.02	-0.39	No
24	17.5	0.02	-0.39	No
25	15.0	0.02	-0.26	Yes
26	12.4	0.02	-0.49	Yes
27	10.0	0.02	-0.58	Yes
28	30.0	0.05	-0.21	No
29	27.4	0.05	-0.11	No
30	25.0	0.05	-0.33	No
31	22.6	0.05	-0.38	No
32	20.0	0.05	-0.42	No
33	17.5	0.05	-0.38	No
34	14.9	0.05	-0.45	Yes
35	12.6	0.05	-0.55	Yes

36	9.9	0.05	-0.61	Yes
37	25.0	0.1	-0.23	No
38	22.4	0.1	-0.39	No
39	20.0	0.1	-0.44	Yes
40	17.4	0.1	-0.46	Yes
41	15.0	0.1	-0.31	Yes
42	12.5	0.1	-0.54	Yes

Liquid film velocities are calculated using Zhang et al. (2003) unified model. The flow conditions correspond to the experimental setups in Yuan (2011) study. Table 2 lists the liquid loading status and the correspondent gas and liquid superficial velocities as well as the liquid film velocities in vertical pipe. Most of liquid loading cases correspond to reversal (downward) film velocities higher than 0.3 m/s, and most of unloading cases occur when the correspondent reversal film velocities are lower than 0.3 m/s. Therefore, the liquid loading onset occurs at a downward (negative) film velocity rather than at the beginning of the film velocity reversal namely zero film velocity.

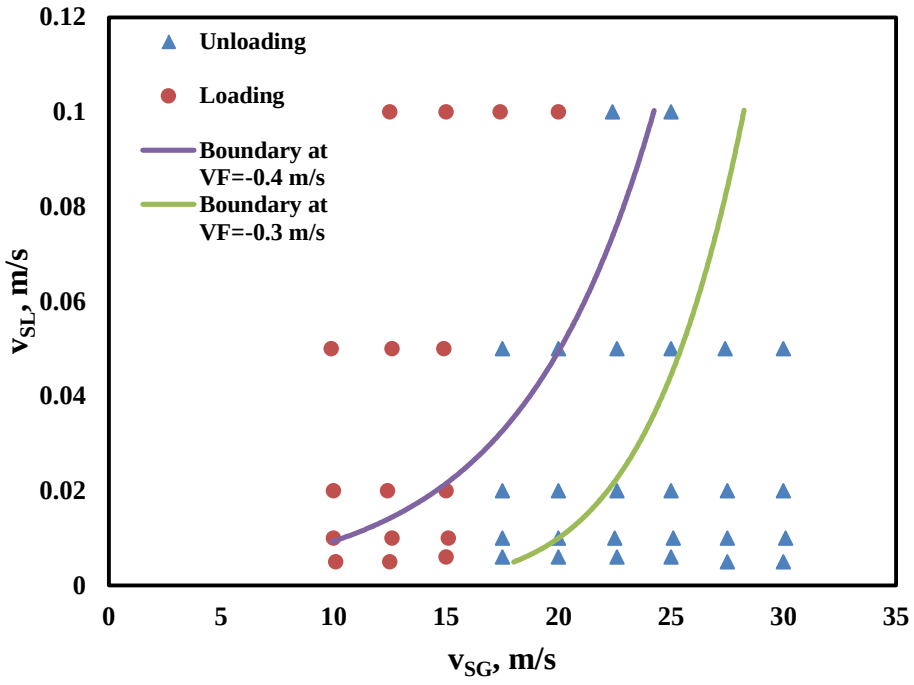

Figure 22: Liquid Loading Onset Related to Film Velocity in Vertical Pipe

As shown in Figure 22, liquid loading and unloading cases are identified on the v_{SL} ~ v_{SG} plane. Two boundaries corresponding to film velocities -0.4 and -0.3 m/s are generated from model simulations. It is seen that the liquid loading onset roughly corresponds to film velocity -0.4 m/s. The critical gas superficial velocity is about 18 m/s.

4.1.2 *Liquid Loading Prediction in 75° Pipe*

Figure 23 shows pressure gradients against superficial gas velocities at different superficial liquid velocities 0.01, 0.05 and 0.1 m/s.

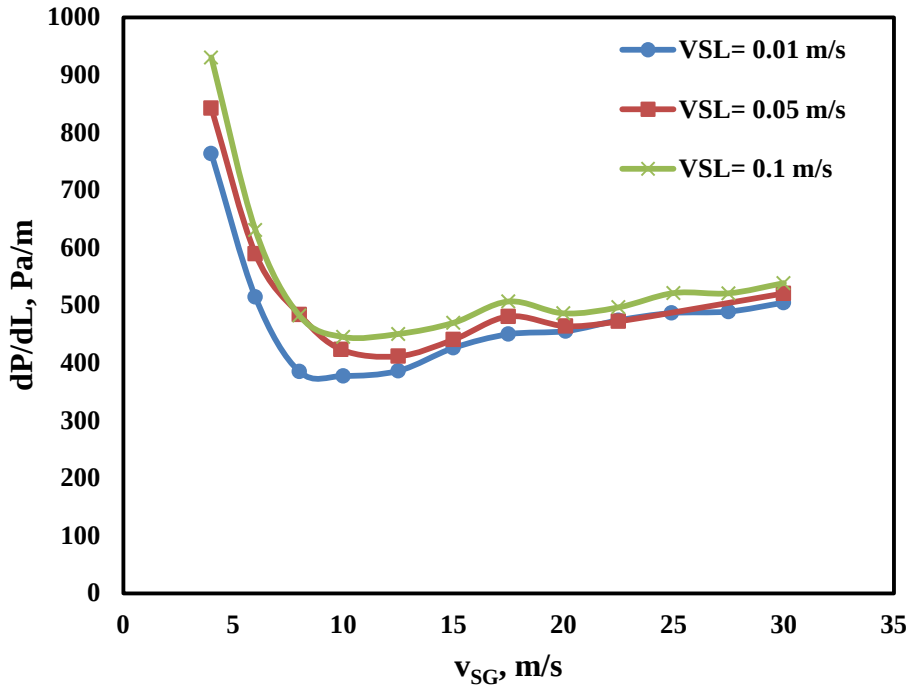

Figure 23: Pressure Gradient vs. Superficial Gas Velocity in 75° Pipe

Compared with vertical pipe flow, similar trends and behavior of pressure gradients in 75° pipe are observed. The critical gas superficial velocities corresponding to the minimum pressure gradients are listed in Table 3.

Table 3: Critical Gas Superficial Velocities at Different Superficial Water Velocities in 75° Pipe

v_{SW}, m/s	v_{SGC}, m/s	$(Dp/dL)_M$, Pa/m	θ, °	Loading
0.01	10.0	377.35	75	Yes
0.05	12.5	411.57	75	Yes
0.10	12.5	450.29	75	Yes

Table 4 lists the liquid loading/unloading status corresponding to different superficial gas and liquid velocities as well as the liquid film velocities in 75° pipe. Film velocities of liquid loading cases vary significantly. However, almost all unloading cases correspond to reverse film velocities lower than 0.3 m/s.

Figure 24 shows liquid loading/unloading cases on the v_{SL} ~ v_{SG} plane. Boundaries corresponding to the same liquid film velocities are also generated with the Zhang et al. unified model. As can be seen, the liquid film velocity of -0.3 m/s is close to the liquid loading onset boundary.

Table 4: Liquid Loading Related to Liquid Film Velocity in 75° Pipe

No.	**v_{SG}**	**v_{SL}**	**v_F**	**Loading or Not**
	m/s	**m/s**	**m/s**	**-**
1	29.9	0.005	-0.13	No
2	27.5	0.006	-0.16	No
3	25.0	0.006	-0.25	No
4	22.5	0.006	-0.30	No
5	20.2	0.006	-0.34	No
6	17.4	0.006	-0.61	Yes
7	15.0	0.005	-0.85	Yes
8	12.5	0.006	-1.08	Yes
9	10.0	0.005	-1.28	Yes
10	30.0	0.01	-0.16	No
11	27.5	0.01	-0.21	No
12	24.9	0.01	-0.18	No
13	22.5	0.01	-0.23	No
14	20.1	0.009	-0.33	No
15	17.5	0.009	-0.61	Yes
16	15.0	0.009	-0.90	Yes
17	12.5	0.009	-1.11	Yes
18	10.0	0.01	-1.33	Yes
19	29.9	0.02	-0.18	No
20	27.5	0.02	-0.22	No

21	25.0	0.02	-0.30	No
22	22.5	0.02	-0.35	No
23	20.0	0.02	-0.38	Yes
24	17.5	0.02	-0.34	Yes
25	15.0	0.02	-0.85	Yes
26	12.5	0.02	-1.11	Yes
27	10.0	0.02	-1.34	Yes
28	30.0	0.05	-0.17	No
29	22.5	0.05	-0.37	No
30	20.1	0.05	-0.41	Yes
31	17.5	0.05	-0.53	Yes
32	15.0	0.05	-0.93	Yes
33	12.5	0.05	-1.12	Yes
34	9.9	0.05	-1.28	Yes
35	30.0	0.1	-0.20	No
36	27.5	0.1	-0.27	No
37	25.0	0.1	-0.23	Yes
38	22.5	0.1	-0.37	Yes
39	20.0	0.1	-0.43	Yes
40	17.5	0.1	-0.53	Yes
41	15.0	0.1	-0.93	Yes
42	12.5	0.1	-1.10	Yes

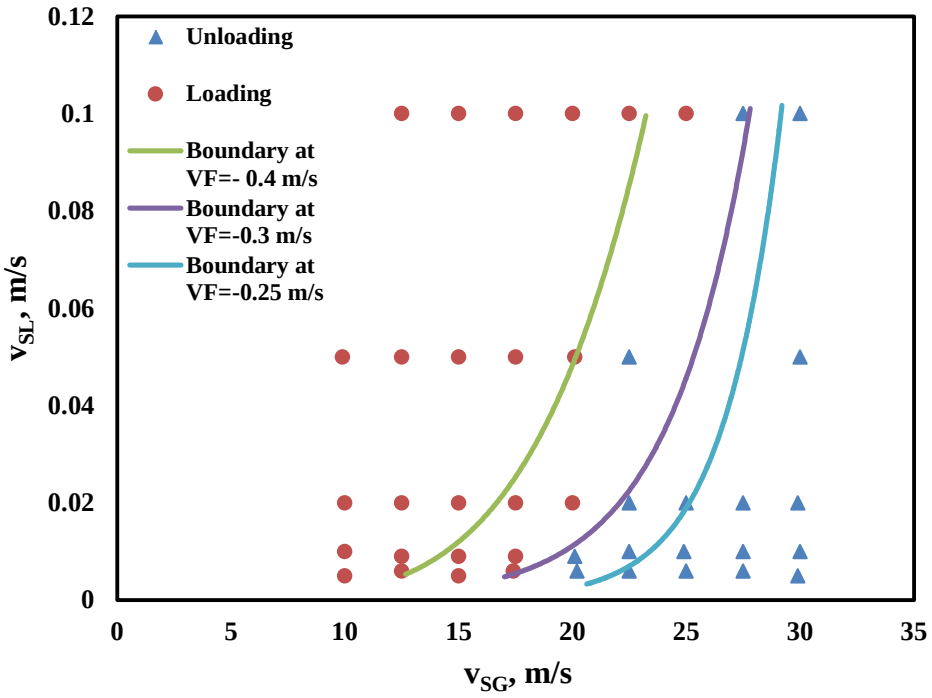

Figure 24: Liquid Loading Onset Related to Film Velocity in 75° Pipe

4.1.3 *Liquid Loading Prediction in 60° Pipe*

Figure 25 shows the pressure gradient changes with superficial gas velocity increase at different superficial liquid velocities in a 60° pipe. The pressure gradient trends are consistent with the 75° pipe and vertical pipe trends. The sharp pressure gradient decreases with gas flow rate increase are corresponding to intermittent flows. The critical gas superficial velocities and the correspondent minimum pressure gradient are listed in Table 5.

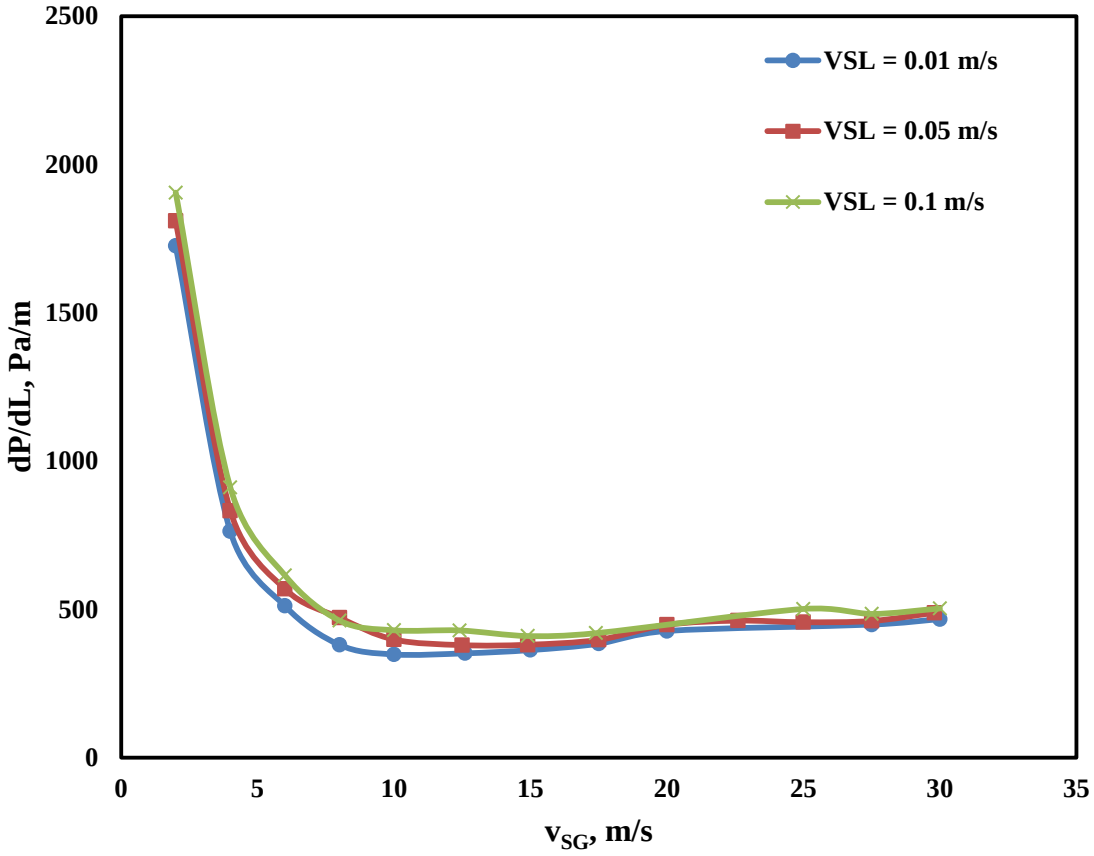

Figure 25: Pressure Gradient vs. Superficial Gas Velocity in 60° Pipe

Table 6 lists the liquid loading and unloading status under different superficial gas and liquid velocities as well as the correspondent liquid film velocities. Most of the liquid loading cases correspond to the reverse liquid film velocity higher than 0.2 m/s.

Table 5: Critical Gas Superficial Velocities at Different Superficial Water Velocities in 60° Pipe

v_{SW}, m/s	v_{SGC}, m/s	$(Dp/dL)_M$, Pa/m	θ, °	Loading
0.01	10.0	348.44	60	Yes
0.05	12.5	379.85	60	Yes
0.10	14.9	410.4	60	Yes

Table 6: Liquid Loading Related to Liquid Film Velocity in 60° Pipe

No.	v_{SG}	v_{SL}	v_F	Loading or Not
	m/s	m/s	m/s	-
1	30.0	0.005	-0.08	No
2	27.5	0.005	-0.06	No
3	24.9	0.005	-0.35	No
4	22.6	0.005	-0.53	No
5	20.0	0.005	-0.72	Yes
6	17.4	0.006	-0.92	Yes
7	15.0	0.006	-1.09	Yes
8	12.5	0.005	-1.26	Yes
9	10.0	0.005	-1.49	Yes
10	30.0	0.01	-0.11	No
11	27.5	0.01	-0.18	No
12	20.0	0.01	-0.75	Yes
13	17.5	0.01	-0.95	Yes
14	15.0	0.01	-1.12	Yes
15	12.6	0.01	-1.31	Yes
16	10.0	0.01	-1.55	Yes
17	30.0	0.02	-0.12	No
18	27.5	0.02	-0.17	No
19	25.0	0.02	-0.38	No
20	22.5	0.02	-0.50	Yes
21	20.0	0.02	-0.42	Yes
22	17.5	0.02	-0.89	Yes
23	15.0	0.02	-1.12	Yes
24	12.6	0.02	-1.32	Yes
25	10.0	0.02	-1.56	Yes
26	29.8	0.05	-0.05	No
27	27.5	0.05	-0.21	Yes
28	25.0	0.05	-0.41	Yes
29	22.6	0.05	-0.50	Yes
30	20.0	0.05	-0.74	Yes
31	17.5	0.05	-0.98	Yes
32	14.9	0.05	-1.15	Yes
33	12.5	0.048	-1.29	Yes

34	30.0	0.1	-0.11	No
35	27.5	0.1	-0.19	Yes
36	25.0	0.1	-0.13	Yes
37	17.4	0.1	-0.99	Yes
38	14.9	0.1	-1.14	Yes
39	12.4	0.1	-1.20	Yes

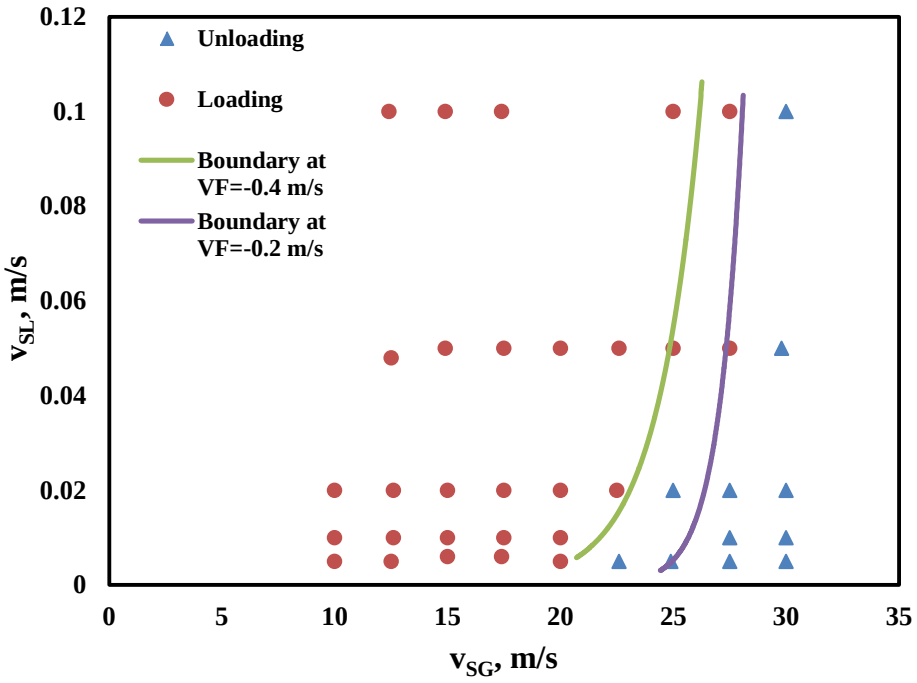

Figure 26: Liquid Loading Onset Related to Film Velocity in 60° Pipe

Figure 26 shows the liquid loading/unloading map on the v_{SL} ~ v_{SG} plane. The two trend lines correspond to two liquid film velocities of -0.2 and -0.4 m/s calculated by the unified model. It appears that the liquid loading onset corresponds to a reverse liquid film velocity 0.2 m/s, which is slightly lower than that in the 75° and vertical pipes.

4.1.4 *Comparison with Experimental Data*

In Table 7, critical gas superficial velocities for liquid loading onset estimated using the minimum pressure gradient method and film velocity reversal method are compared with critical gas superficial velocities observed in the experimental study from Yuan (2011). The comparison shows that the overall critical gas superficial velocities estimated with the minimum pressure gradient method have larger discrepancies from the experimental data. Liquid film reversal is a better indicator of liquid loading onset.

Table 7: Liquid Loading Onsets Predicted by Minimum Pressure Gradient Method and Film Reversal Method Compared with Experimental Observations

v_{SL}, m/s	$v_{SG, exp}$ m/s	$v_{SG, dP/dL}$ m/s	$v_{SG, film\ velocity}$ m/s	θ, °	dP/dL, Discrepancy	v_F, Discrepancy
0.01	15.1	10.0	18.0	90	34%	19%
0.05	14.9	12.6	15.8	90	15%	6%
0.10	20.0	17.4	22.5	90	13%	13%
0.01	17.5	10.0	21.0	75	43%	20%
0.05	20.1	12.5	26.0	75	38%	29%
0.10	25.0	12.5	24.0	75	50%	4%
0.01	20.0	10.0	25.0	60	50%	25%
0.05	27.5	12.5	25.8	60	55%	6%
0.10	27.5	14.9	26.2	60	46%	5%

Intuitively, liquid loading onset should correspond to liquid film velocity zero, since liquid film reverse flow will cause liquid accumulation in a well. However, the model simulated liquid film velocities corresponding to the liquid loading onset shown in Figures 22, 24 and 26 are around -0.3 m/s for flows in vertical, 75° and 60° pipes. This means the liquid entrained in the gas core area is even higher than the liquid flow rate.

In Yuan (2011) experiments, the movement of gas bubbles in liquid film was observed to represent liquid film velocity. However, slippage exists between gas bubbles and liquid film. Therefore, the gas bubble velocity observed in the experiment is the slippage velocity plus the film velocity (Figure 27):

$$v_B = v_F + v_S \tag{5.1}$$

v_S is slippage velocity, m/s. v_B is the gas bubble velocity in the liquid film, m/s. v_F is the liquid film velocity along the tubing, m/s.

Harmathy (1960) proposed a correlation to calculate slippage velocity, which is also called bubble-rise velocity:

$$v_S = 1.53\left[\frac{g\sigma_L(\rho_L - \rho_G)^{1/4}}{\rho_L^2}\right] \tag{5.2}$$

σ_L is liquid-gas interfacial tension, N/m. With gas and liquid properties, the slippage velocity between the gas bubbles and liquid film can be obtained, which is summarized in Table 8.

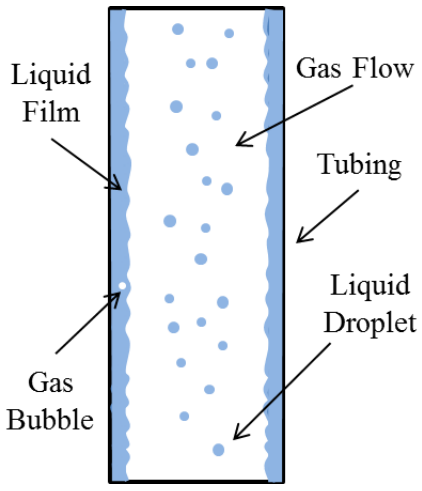

Figure 27: Slippage between Gas Bubble and Liquid Film

As can be seen from Table 8, the calculated slippage velocity is 0.25 m/s based on Harmathy (1960) model. Accordingly in a vertical pipe, if the observed bubble velocity is 0, the liquid film is likely flowing downward with a velocity of -0.25 m/s. Therefore, the liquid loading onset boundary should correspond to a film velocity of about -0.25 m/s which is close to the model predictions.

Table 8: Fluid Properties and Slippage Velocity

Fluid Properties		**Slippage**	
g, m/s^2	9.81	**v_S, m/s**	0.25
ρ_L, kg/m^3	998.0		
ρ_G, kg/m^3	1.27		
σ_L, N/m	0.073		

Liquid droplets are entrained from liquid film by the gas core and flow upward. Part of the liquid droplets deposit on the liquid film. The entrainment of liquid droplets exceeds the liquid flow rate when liquid film flows downward. This phenomenon also explains that although liquid loading may occur at the bottom hole, some liquid is still carried to the wellhead.

More simulations are carried out with the Zhang et al. (2003) unified model. Figure 28 shows the calculated trends of film velocities with varying superficial gas velocity at superficial liquid velocities 0.005, 0.05 and 0.1 m/s in vertical, 75° and 60° pipes.

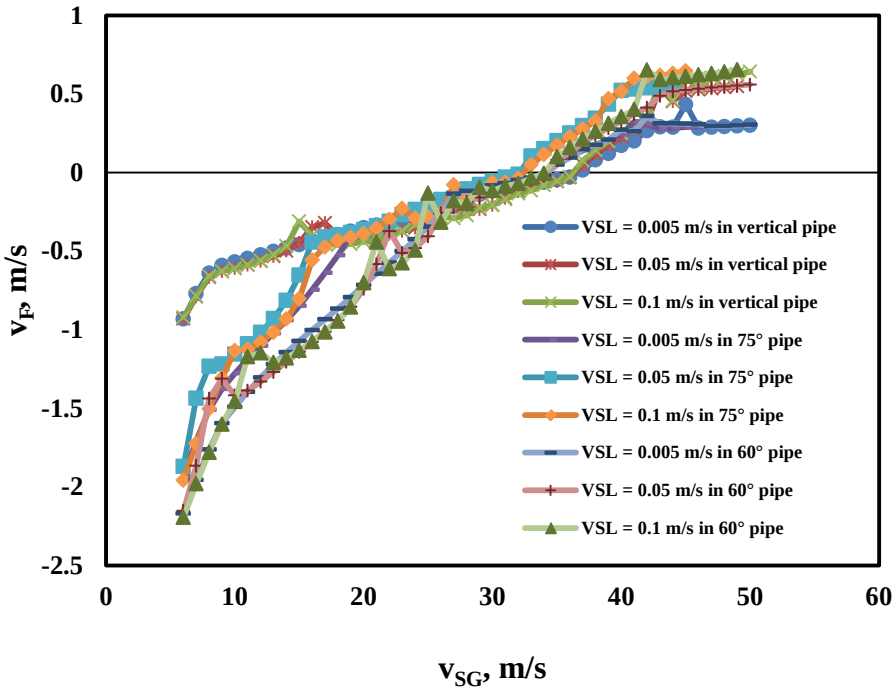

Figure 28: Liquid Film Velocity vs. Superficial Gas Velocity at Superficial Liquid Velocities 0.005, 0.05 and 0.1 m/s in Vertical, 75° and 60° Pipes

Film velocity increases from negative value to positive value as superficial gas velocity increases. At low gas flow rate, gas flow is unable to carry liquid film upward. Liquid flows upward as liquid slugs or big waves supported by gas flow. With gas velocity increase the liquid film downward velocity becomes lower and the liquid holdup sharply decreases. As a result, liquid accumulation is reduced and the well is unloaded. When gas velocity is further increased, liquid film will turn around and flow upward. The liquid holdup becomes very low and gravitational pressure gradient is small compared to frictional pressure gradient.

4.2 Plunger Lift Model Simulation Results

In this section, the new plunger lift model simulation results are presented and discussed. Water and oil case studies are conducted. Simulation results are compared with predictions of previous models.

4.2.1 Water Case

The water case inputs are from Lea (1982) and Gasbarri and Wiggins (2001) studies as listed in Appendix A.

Table 9: Water Case Study Results

Gas Production Rate, SCF/D	897,657.0
Liquid Production Rate, STB/D	141.2
Minimum Casing Pressure, psig	185.5
Maximum Casing Pressure, psig	1,944.5
Minimum Tubing Pressure, psig	216.6
Maximum Tubing Pressure, psig	2,320.0
Cycles per Day	18.2
Average Upstroke Velocity, ft/min	2,772.6
Slug Surface Arrival Time, s	92.0
Plunger Surface Arrival Time, s	101.0
Blowdown Time, s	3,600.0
Build Up Time, s	958.0
Build Up Casing Pressure, psig	1,031.0

The base input parameters are borrowed from Lea case study and Gasbarri and Wiggins case study. The rest required information is assumed from industry experience. The assumed simulation inputs lead to significant difference in the simulation results

from the original cases. Thus, in the new model case study, the main objective is to verify the trends, rather than the quantitative values.

Simulation results of the water case are shown in Table 9. Gas production rate is 897,657.01SCF/D and liquid production rate is 141.15 STB/D. Plunger lift build-up time, 958.0 s, and blowdown time, 3600.0 s, are determined by reservoir performance and liquid accumulation, respectively. The time cycle, 4747.0 s, is much longer than 1250.0 s presented by Gasbarri and Wiggins case study. The longer time cycle may be due to different reservoir characteristics used in the water case study. Additional figures of plunger lift water case are shown in Appendix A.

In the present model the calculation of gas section part has been improved compared to the Gasbarri and Wiggins model. Figure 29 shows the comparison of the new model predicted gas flow rate (in gas section) with Gasbarri and Wiggins model prediction. The Gasbarri and Wiggins model (red line) predicts a gas velocity about 810.6 m/s at the peak, which is much higher than the local sound speed 421.9 m/s.

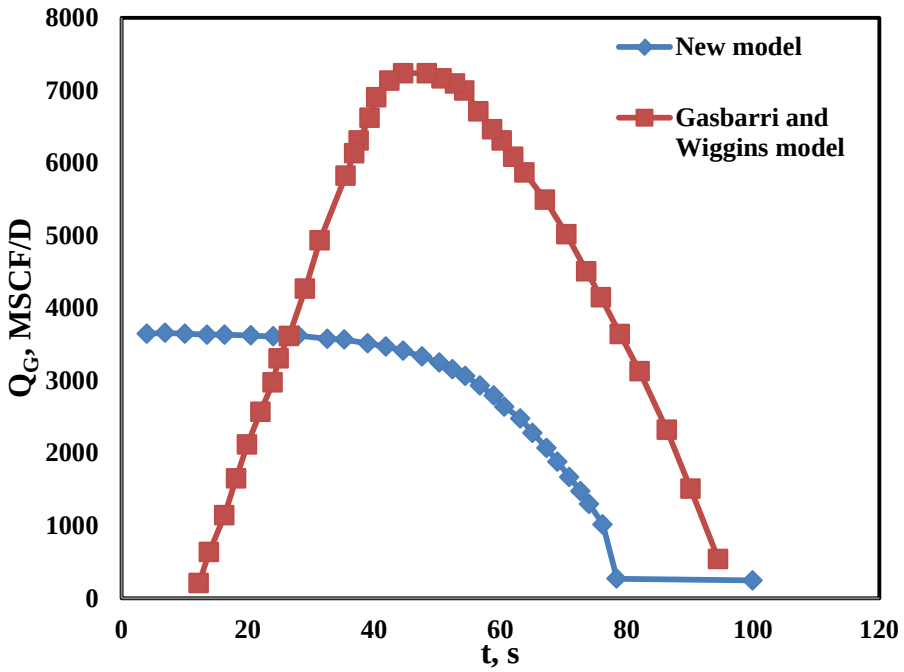

Figure 29: Gas Flow Rate Comparison above Liquid Slug for Water Case

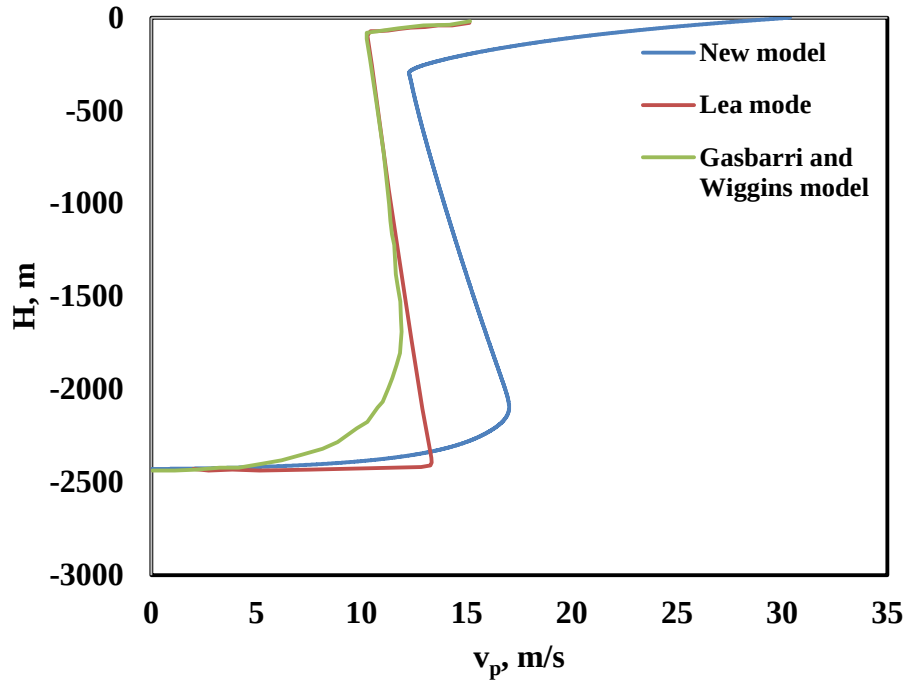

Figure 30: Plunger Velocity vs. Well Depth for Water Case

In our new plunger lift model, the unrealistic over prediction of the gas flow rate in the previous model has been improved. If local gas velocity reaches the sound speed, the gas flow rate in the new model is kept constant. This is why a big difference between the new model and the Gasbarri and Wiggins model is observed in Figure 29.

Figure 30 shows the plunger velocity versus well depth predicted by the new model compared with Lea model and Gasbarri and Wiggins model. Similar trends are predicted by the previous models and the present model, although the reservoir depth and productivity of the current water case are higher. From bottomhole, plunger velocity increases (acceleration) due to reservoir pressure energy exerted on plunger and liquid slug. After plunger velocity reaches the maximum value, its velocity decreases gradually because of gravity. After liquid slug arrives at the surface, plunger velocity increases again due to the pressure difference increase between upstream and downstream of the plunger.

The plunger velocity curve (blue curve) predicted by the new model is smoother compared with Lea model prediction which gives sharp turning points at the transitions between different stages. The difference is due to that Lea model is a static model while the new model is a dynamic model.

Figure 31 presents plunger velocity change with time for the entire working cycle. The red curve denotes Gasbarri and Wiggins model prediction and the blue curve is the prediction of the new model in this study. Plunger velocity increases at beginning corresponding to the plunger upstroke process. Then, plunger velocity remains zero for a certain period of time for blowdown. The new model has longer blowdown time, while Gasbarri and Wiggins model has much shorter blowdown time.

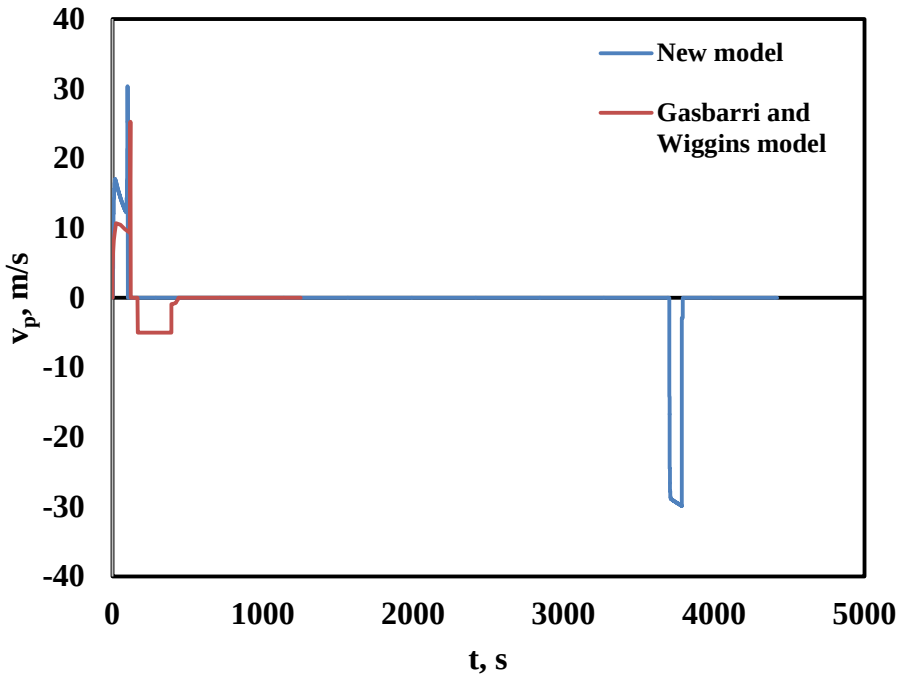

Figure 31: Plunger Velocity Corresponding to Plunger Depth for Water Case

The negative plunger velocity corresponds to the downstroke phase. As shown by the blue curve, plunger falls down in the tubing with high velocity in the gas phase. Due to gravity effect, plunger falling velocity increases gradually with time. When the plunger enters in liquid phase, its falling velocity decreases becasue of buoyancy and resistance of liquid. Finally, plunger falling velocity returns to zero when it hits the bottom seat and starts the the buildup phase. In the Gasbarri and Wiggins case study (red curve), obviously, the plunger falling velocity was constant at 1000 ft/min in gas phase and 175 ft/min in liquid phase.

4.2.2 *Oil Case*

The detailed input parameters for the oil case study are listed in Appendix A. Some of these parameters are from Lea (1982) oil case study. The other required inputs are assumed based on a typical high GOR oil well production. Table 10 summarizes simulation results of the oil case. Compared with Gasbarri Wiggins model simulation results and field data indicated from Lea paper and Gasbarri and Wiggins paper, these values are reasonable. Additional figures of plunger lift oil case are shown in Appendix A.

Table 10: Oil Case Study Results

Gas Production Rate, SCF/D	419,877.5
Liquid Production Rate, STB/D	77.1
Minimum Casing Pressure, psig	158.8
Maximum Casing Pressure, psig	1,678.8
Minimum Tubing Pressure, psig	185.3
Maximum Tubing Pressure, psig	1,999.5
Cycles per Day	32.2
Average Upstroke Velocity, ft/min	3,138.9
Slug Surface Arrival Time, s	85.0
Plunger Surface Arrival Time, s	90.0
Blowdown Time, s	1,848.0
Build Up Time, s	554.0
Build Up Casing Pressure, psig	628.0

Figure 32 shows the plunger velocity change with well depth for the oil case study. Compared to water case study, similar plunger velocity trends are obtained. The big difference appeared in the new model prediction is due to small volume of liquid slug above the plunger. Because of the small resistance and different reservoir performance functions used in those models where productivity methods are used in the new model

and the backpressure method is employed in the Gasbarri and Wiggins model, high plunger acceleration is generated by the pressure energy under the plunger from reservoir. Thus, plunger upstrokes velocity increases very quickly because of the high plunger acceleration. High gas production rate from reservoir also contributes to this difference.

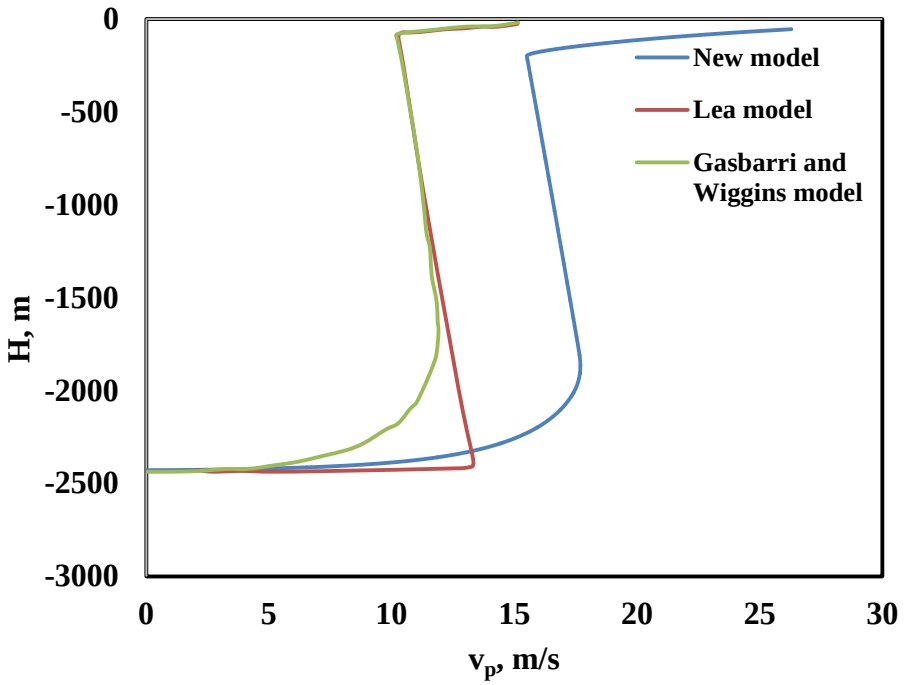

Figure 32: Plunger Velocity for Oil Case

Figure 33 presents plunger velocity changes with time for the oil case. The trends are similar as that of the water case. Compared with Gasbarri and Wiggins case study, the new oil case has longer blowdown and build up time due to different reservoir properties used in the case study which Gasbarri and Wiggins did not provide. The previous model assumed constant plunger falling velocities in both gas and liquid phases. The new model considers plunger falling acceleration in down stroke.

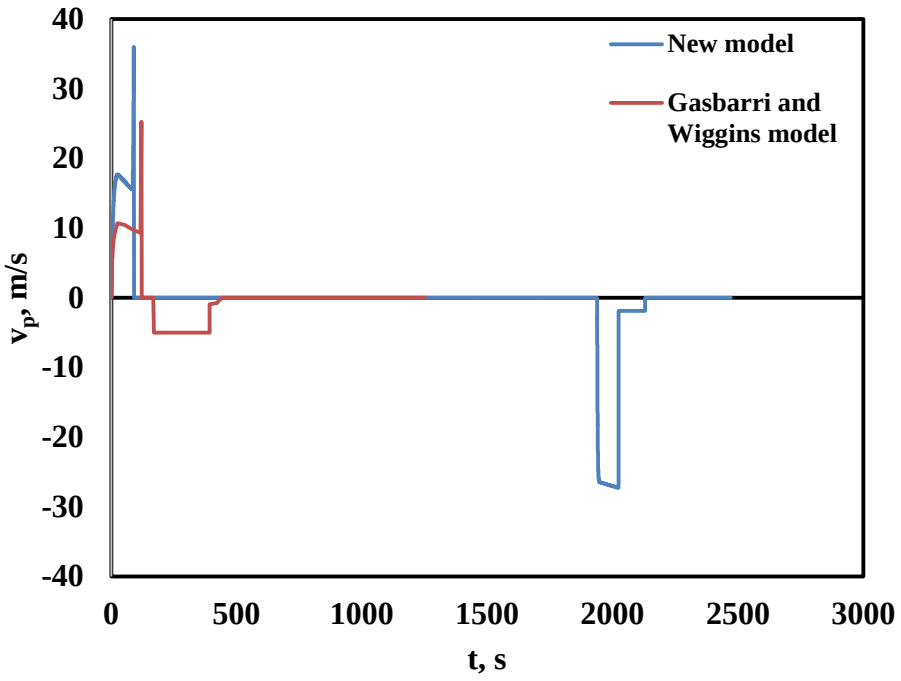

Figure 33: Plunger Velocity vs. Time for Oil Case

CHAPTER 5

CONCLUSIONS AND RECOMMENDATIONS

5.1 Summary and Conclusions

5.1.1 Liquid Loading Onset

After analyzing the mechanistic model simulation results and comparing with previous experimental data, several conclusions can be made:

1. Liquid loading onset in gas well is analyzed through simulations using Zhang et al. (2003) unified model for gas-liquid flows in vertical, 75° and 60° pipes. Comparing with experimental data from Yuan (2011), the simulation results indicate that liquid loading onset corresponds to a reverse liquid film velocity around 0.3 m/s. This is contradictory to the common understanding that liquid loading starts at the beginning of liquid film reversal.
2. In Yuan (2011) experiments, liquid film flow direction was traced by gas bubbles in liquid film. A slippage velocity about 0.25 m/s exists between liquid film and gas bubbles. Therefore, stagnant gas bubbles are likely corresponding to a downward film velocity about 0.25 m/s, which is close to that observed in the model simulations.

5.1.2 Plunger Lift Modeling

1. A new plunger lift model is developed in this study, combining advantages of the Gasbarri and Wiggins model (2001) and Lea model (1982). A plunger lift simulator is also programmed using Visual Basic.
2. Instead of using the constant plunger falling velocities in the tubing, the new model calculates plunger falling velocity in the downstroke phase based on plunger gravity and drag force balance.
3. The present model restricts the unreasonable prediction of gas flow rate above the plunger in upstroke phase within the gas flow rate corresponding to the local sound speed.

5.2 Recommendations

1. In this study, the new model is compared with simulation results of other existing plunger lift models. The new closure relationships used in the new model need to be verified with experimental results. For example, plunger falling experiments can be conducted to validate the plunger acceleration and drag coefficients.
2. Liquid leakage between plunger and tubing during the plunger travelling in the tubing needs to be included in the plunger lift model. New model of liquid leakage should be developed in future study.
3. Additional field data from industry will help improve the prediction accuracy of the proposed plunger lift model by fine tuning the new closure relationships.

NOMENCLATURE

Symbol	Description
a_L	acceleration in surface pipeline
A_L	pipeline cross sectional area
$A_{projected}$	projected area
a_t	acceleration in tubing
A_{tubing}	tubing cross section area
C_d	drag coefficient
C_t	total compressibility
d_L	pipe diameter
$D_{plunger}$	plunger diameter
d_T	tubing diameter
E_k	kinetic energy
f_L	liquid friction factor for surface pipeline
f_l	liquid friction factor for tubing
g	gravitational acceleration
h	thickness of pay zone
H_L	liquid holdup
H_{LF}	liquid film holdup
H_{LS}	slug liquid holdup
k	permeability

l_F	film length
L_L	length of pipeline
L_t	slug length in tubing
$m_{l,L}$	liquid mass in surface pipeline
$m_{l,t}$	liquid mass in tubing
$m_{particle}$	mass of falling particle
$m_{plunger}$	mass of plunger
p_1	pressure below the plunger
p_2	pressure above liquid slug in tubing
p_3	pressure at front of slug in pipeline
P_e	reservoir pressure
P_{SC}	standard condition pressure
P_w	bottomhole pressure
r_e	drainage radius
R_e	drainage radius
R_w / r_w	wellbore radius
T	temperature
T_{SC}	standard condition temperature
$u_{l,L}$	control volume velocity in surface pipeline
$u_{l,t}$	control volume velocity in tubing
v_C	gas core velocity
VF	film velocity
v_F	film velocity

v_G	gas velocity
$v_{gas\text{-}bubble}$	gas bubble velocity in liquid film
$v_{l,L}$	liquid velocity in surface pipeline
$v_{l,t}$	liquid velocity in tubing
$v_{liquid\text{-}film}$	liquid film velocity in tubing
$v_{plunger}$	plunger velocity
v_{SG}	superficial gas velocity
v_{SL}	superficial liquid velocity
v_{slip}	slip velocity
v_{SW}	superficial water velocity
v_T	slug translational velocity
v_t	terminal velocity
$v_{t\text{-}turner}$	terminal velocity from Turner et al.
$v_{t\text{-}zhou}$	terminal velocity from Zhou et al.
w	mass of liquid slug
Z	gas compressibility factor
Z_{SC}	gas compressibility factor at standard condition

Greek Letters

Symbol	**Description**
α	coefficient from Zhou et al.
β	coefficient from Zhou et al.
κ	empirical friction factor of tee section

μ	viscosity
θ	inclination angle
ρ	density
ρ_G	gas density
$\rho_{g,SC}$	gas density at standard condition
ρ_L	liquid density
ρ_l	liquid slug density
$\rho_{particle}$	density of particle
σ_L	gas-liquid interfacial tension

BIBLIOGRAPHY

[1] Alsaadi, Y. 2013. Liquid loading in highly deviated gas wells. M.S. Thesis, The University of Tulsa.

[2] Andrade, J., Jimenez, J.L., and Parada, M.S.M. 2013. Mature fields, oil well optimization using plunger lift systems in Tibu Field. SPE Artificial Lift Conference-Americas. Society of Petroleum Engineers. SPE-165056-MS.

[3] Bahadori, A., Zahedi, G., Zendehboudi, S., and Jamili, A. 2012. A simple method to estimate the maximum liquid production rate using plunger lift system in wells. *Nafta* 63(11-12): 365-369.

[4] Barnea, D. 1987. A unified model for predicting flow-pattern transitions for the whole range of pipe inclinations. *International Journal of Multiphase Flow* 13(1): 1-12.

[5] Baruzzi, J.O.A., and Alhanati, F.J.S. 1995. Optimum plunger lift operation. SPE Production Operations Symposium. Society of Petroleum Engineers. SPE-29455-MS.

[6] Belfroid, S., Schiferli, W., Alberts, G., Veeken, C.A., and Biezen, E. 2008. Prediction onset and dynamic behavior of liquid loading gas wells. In SPE Annual Technical Conference and Exhibition. Society of Petroleum Engineers. SPE-180403-MS.

[7] Charcin U.J.E. 1990. Modeling and optimization of intermittent gas-plunger lift installations. Project Report, University of Tulsa.

[8] Chava, G., Falcone, G., and Teodoriu, C. 2010. Plunger-lift modeling toward efficient liquid unloading in gas wells. SPE Projects, *Facilities & Construction* 5(01): 38-45. SPE-124515-PA.

[9] Chava, G.K., Falcone, G., and Teodoriu, C. 2008. Development of a new plunger-lift model using smart plunger data. SPE Annual Technical Conference and Exhibition. Society of Petroleum Engineers. SPE-115934-MS.

[10] Coleman, S.B., Clay, H.B., McCurdy, D.G., and Norris III, L.H. 1991. A new look at predicting gas-well load-up. *Journal of Petroleum Technology* 43(03): 329-333.

[11] Fernandez, J.J., Falcone, G., and Teodoriu, C. 2010. Design of a high-pressure research flow loop for the experimental investigation of liquid loading in gas wells. *SPE Projects, Facilities & Construction* 5(02): 76-88. SPE-122786-PA.

[12] Fiedler, S., and Auracher, H. 2004. Experimental and theoretical investigation of reflux condensation in an inclined small diameter tube. *International Journal of Heat and Mass Transfer* 47(19): 4031-4043.

[13] Flores-Avila, F.S., Smith, J.R., Bourgoyne Jr, A.T., and Bourgoyne, D.A. 2002. Experimental evaluation of control fluid fallback during off-bottom well control: effect of deviation angle. IADC/SPE Drilling Conference. Society of Petroleum Engineers. SPE-74568-MS.

[14] Foss, D.L., and Gaul, R.B. 1965. Plunger-life performance criteria with operating experience – Ventura Avenue Field. Drilling and Production Practice. American Petroleum Institute. API-65-124.

[15] Garg, D.O., Lea, J.F., Oetama, T.P., and Cox, J.C. 2005. New considerations for modeling plunger performance. SPE Production Operations Symposium. Society of Petroleum Engineers. SPE-93997-MS.

[16] Gasbarri, S., and Wiggins, M.L. 2001. A dynamic plunger lift model for gas wells. *SPE production & Facilities*, 16(02) 89-96. SPE-72057-PA.

[17] Gawas, K. 2013. Studies in low-liquid loading in gas/oil/water three phase flow in horizontal and near-horizontal pipes. Ph.D. Dissertation, The University of Tulsa.

[18] Girija, E.G. 2006. Experimental study of gas-liquid flow through a tubing-casing annulus with application to natural gas wells. M.S. Thesis, Colorado School of Mines.

[19] Girija, E.G., Christiansen, R.L, and Miller, M.G. 2007. Experimental study of critical flow rates in the tubing-casing annulus of natural-gas wells. SPE Annual Technical Conference and Exhibition. Society of Petroleum Engineers. SPE-109609-MS.

[20] Guner, M. 2012. Liquid loading of gas wells with deviations from 0° to 45°. M.S. Thesis, The University of Tulsa.

[21] Guo, B., Ghalambor, A., and Xu, C. 2005. A systematic approach to predicting liquid loading in gas wells. SPE Production Operations Symposium. Society of Petroleum Engineers. SPE-94081-MS.

[22] Hassouna, M. 2013. Plunger lift applications: Challenges and economics. North Africa Technical Conference and Exhibition. Society of Petroleum Engineers. SPE-164599-MS.

[23] Hearn, W.J., Morrow, S., and Cisneros, R. 2006. New techniques for plunger lift in conventional and nonconventional gas. SPE Eastern Regional Meeting. Society of Petroleum Engineers. SPE-104556-MS.

[24] Hinze, J.O. 1955. Fundamentals of the hydrodynamic mechanism of splitting in dispersion processes. *AIChE Journal* 1(3): 289-295.

[25] Kravits, M.S., Frear, R.M., and Bordwell, D. 2011. Analysis of plunger lift applications in the Marcellus shale. SPE Annual Technical Conference and Exhibition. Society of Petroleum Engineers. SPE-147225-MS.

[26] Lea, J.F. 1982. Dynamic analysis of plunger lift operations. *Journal of Petroleum Technology* 34(11): 2-617.

[27] Lea, J.F. 1999. Plunger lift versus velocity strings. *Journal of Energy Resources Technology* 121(4): 234-240.

[28] Marcano, L., and Chacín, J. 1994. Mechanistic design of conventional plunger lift installations. *SPE Advanced Technology Series* 2(01): 15-24. SPE-23682-PA.

[29] Mirazizi, H. 2015. Low liquid loading three-phase flow and effect of MEG on flow behavior. Ph.D. Dissertation, The University of Tulsa.

[30] Morrow, S.J., and Hearn, W.J. 2007. Plunger-lift advancements, including velocity and pressure analysis. Latin American & Caribbean Petroleum Engineering Conference. Society of Petroleum Engineers. SPE-108104-MS.

[31] Mower, L.N., Lea, J.F., Beauregard, E., and Ferguson, P.L. 1985. Defining the characteristics and performance of gas-lift plungers. SPE Annual Technical Conference and Exhibition. Society of Petroleum Engineers. SPE-14344-MS.

[32] Nadkrynechny, R., Rowlan, O.L., Cepuch, C., Lea, J.F., and McCoy, J.N. 2013. Measured plunger fall velocity used to calibrate new fall velocity model. SPE Production and Operations Symposium. Society of Petroleum Engineers. SPE-0713-0094-JPT.

[33] Nallaparaju, Y.D. 2012. Prediction of liquid loading in gas wells. SPE Annual Technical Conference and Exhibition. Society of Petroleum Engineers. SPE-155356-MS.

[34] Neves, T.R., and Brimhall, R.M. 1989. Elimination of liquid loading in low-productivity gas wells. SPE Production Operations Symposium. Society of Petroleum Engineers. SPE-18833-MS.

[35] Nosseir, M.A., Darwich, T.A., Sayyouh, M.H., and El Sallaly, M. 1997. A new approach for accurate prediction of loading in gas wells under different flowing conditions. SPE Production Operations Symposium. Society of Petroleum Engineers. SPE-66540-PA.

[36] Oyewole, P.O., and Garg, D.O. 2007. Plunger lift application and optimization in San Juan North Basin – Our journey. Production and Operations Symposium. Society of Petroleum Engineers. SPE-106761-MS.

[37] Parsa, E.E., Ozkan, E., Lohmann, M., Cathcart, D., and Lowrey, B. 2013. Enhanced plunger lift performance utilizing reservoir modeling. SPE Production and Operations Symposium. Society of Petroleum Engineers. SPE-164473-MS.

[38] Rawlins, E, L, and Schellhardt, M, A. 1935. *Back-pressure data on natural-gas wells and their application to production practices*. No. BM-Mon-7. Bureau of Mines, Bartlesville, Okla.(USA).

[39] Rowlan, O.L., McCoy, J.N., and Podio, A.L. 2006. Analyzing and troubleshooting plunger-lifted wells. SPE Annual Technical Conference and Exhibition. Society of Petroleum Engineers. SPE-102336-MS.

[40] Schmitz, R., and Steele, G. 2006. Combining plunger lift and compression to lift liquids in low rate gas wells. Canadian International Petroleum Conference. Petroleum Society of Canada. PETSOC-2006-159.

[41] Solomon, F.A., Falcone, G., and Teodoriu, C. 2008. Critical review of existing solutions to predict and model liquid loading in gas wells. SPE Annual Technical Conference and Exhibition. Society of Petroleum Engineers. SPE-115933-MS.

[42] Sutton, R.P., Cox, S.A., Lea, J.F., and Rowlan, O.L. 2010. Guidelines for the proper application of critical velocity calculations. *SPE Production & Operations* 25(02): 182-194. SPE-120625-PA.

[43] Taitel, Y., Bornea, D., and Dukler, A.E. 1980. Modelling flow pattern transitions for steady upward gas-liquid flow in vertical tubes. *AIChE Journal* 26(3): 345-354.

[44] Tang, Y., and Liang, Z. 2008. A new method of plunger lift dynamic analysis and optimal design for gas well deliquification. SPE Annual Technical Conference and Exhibition. Society of Petroleum Engineers. SPE-116764-MS.

[45] Toma, P., Vargas, E., and Kuru, E. 2006. Prediction of slug-to-annular flow pattern transition (SAT) for reducing the risk of gas lift instabilities and effective gas-liquid transport from low-pressure reservoirs. SPE Gas Technology Symposium. Society of Petroleum Engineers. SPE-100615-MS.

[46] Turner, R.G., Hubbard, M.G., and Dukler, A.E. 1969. Analysis and prediction of minimum flow rate for the continuous removal of liquids from gas wells. *Journal of Petroleum Technology* 21(11): 1-475.

[47] van't Westende, J.M.C. 2008. Droplets in annular-dispersed gas-liquid pipe-flows. Ph.D. Dissertation, Delft University of Technology, Netherlands.

[48] van't Westende, J.M.C., Kemp, H.K., Belt, R.J., Portela, L.M., Mudde, R.F., and Oliemans, R.V.A. 2007. On the role of droplets in co-current annular and churn-annular pipe flow. *International Journal of Multiphase Flow* 33(6): 595-615.

[49] Veeken, C.A., Hu, B., and Schiferli, W. 2009. Transient multiphase flow modeling of gas well liquid loading. Society of Petroleum Engineers. SPE-123657-MS.

[50] Yuan, G. 2011. Liquid loading of gas wells. M.S. Thesis, The University of Tulsa.

[51] Zabaras, G., Dukler, A.E., and Moalem-Maron, D. 1986. Vertical upward cocurrent gas-liquid annular flow. *AIChE Journal* 32(5): 829-843.

[52] Zhang, H.-Q., Wang, Q., Sarica, C., and Brill, J.P. 2003. Unified model for gas-liquid pipe flow via slug dynamics—part 1: model development. *Journal of Energy Resources Technology* 125(4): 266-273.

[53] Zhang, H.-Q., Wang, Q., Sarica, C., and Brill, J.P. 2003. Unified model for gas-liquid pipe flow via slug dynamics—part 2: model validation. *Journal of Energy Resources Technology* 125(4): 266-273.

[54] Zhou, D., and Yuan, H. 2009. New model for gas well loading prediction. SPE Production and Operations Symposium. Society of Petroleum Engineers. SPE-120580-MS.

[55] Zhu, J., and Zhang, H.-Q. 2014. CFD simulation of ESP performance and bubble size estimation under gassy conditions. SPE Annual Technical Conference and Exhibition. Society of Petroleum Engineers. SPE-170727-MS.

APPENDIX A

ADDITIONAL TABLES

The input parameters for case studies are listed in the following tables.

Table 11: Well Geometry for Water Case

Well Depth, m	2428	Plunger OD, m	0.073
Tubing ID, m	0.075	Plunger Mass, kg	20
Tubing OD, m	0.077	Plunger Type	Casing to Tubing
Casing ID, m	0.1		

Table 12: Surface Parameters for Water Case

Surface Line Length, m	50
Surface Line ID, m	0.075
Separator Pressure, MPa	1.2

Table 13: Reservoir Parameters for Water Case

Pore Pressure, MPa	16	Surface Temperature, K	293
Gas Permeability, mD	100	Well Diameter, m	0.216
Reservoir Thickness, m	10	Liquid Gas Ratio	0.00002
Drainage Radius, m	50	Coefficient *C*	0.84
Geothermal Gradient, K/m	0.03	Exponent *n*	1.34

Table 14: Fluid Properties for Water Case

Liquid Density, kg/m^3	1000
Gas Specific Density	0.60
Initial Slug Length, m	300

Table 15: Well Geometry for Oil Case

Well Depth, m	2428	Plunger OD, m	0.05
Tubing ID, m	0.051	Plunger Mass, kg	5
Tubing OD, m	0.06	Plunger Type	Casing to Tubing
Casing ID, m	0.116		

Table 16: Surface Parameters for Oil Case

Surface Line Length, m	50
Surface Line ID, m	0.051
Separator Pressure, MPa	0.41

Table 17: Fluid Properties for Oil Case

Liquid Density, kg/m^3	860
Gas Specific Density	0.6
Initial Liquid Length, m	200

Table 18: Reservoir Parameters for Oil Case

Pore Pressure, MPa	13.79	Surface Temperature, K	293.15
Gas Permeability, mD	80	Well Diameter, m	0.216
Reservoir Thickness, m	15.24	Liquid Gas Ratio	0.00002
Drainage Radius, m	358.9	Coefficient *C*	0.84
Geothermal Gradient, K/m	0.03	Exponent *n*	1.34

Table 19: Special Parameter for Water and Oil Case

Absolute Roughness, m	0.00025

ADDITIONAL FIGGURES FOR WATER CASE AND OIL CASE

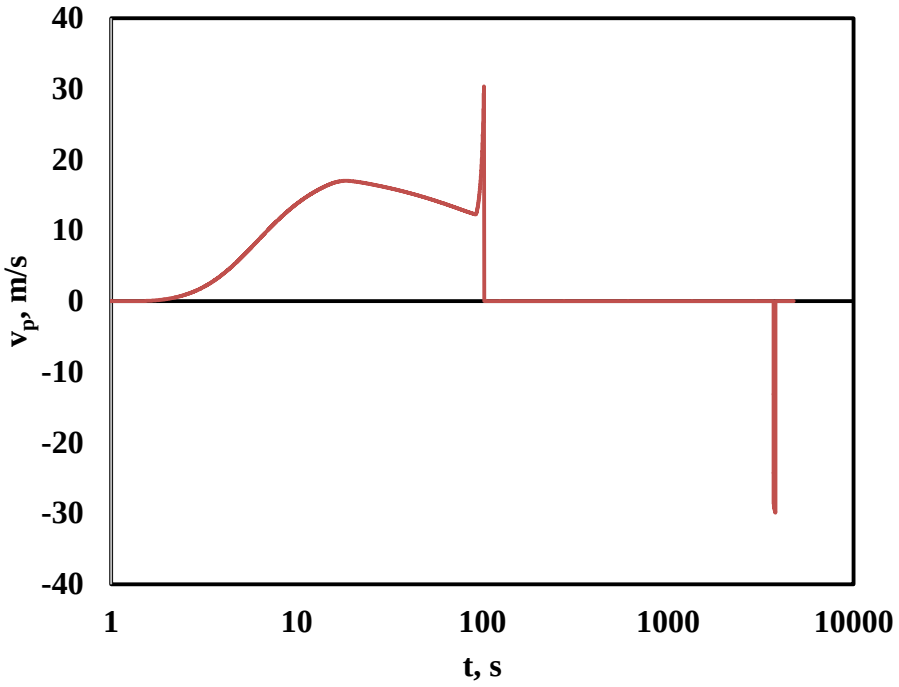

Figure 34: Plunger Velocity vs. Time for Entire Cycle (Water Case)

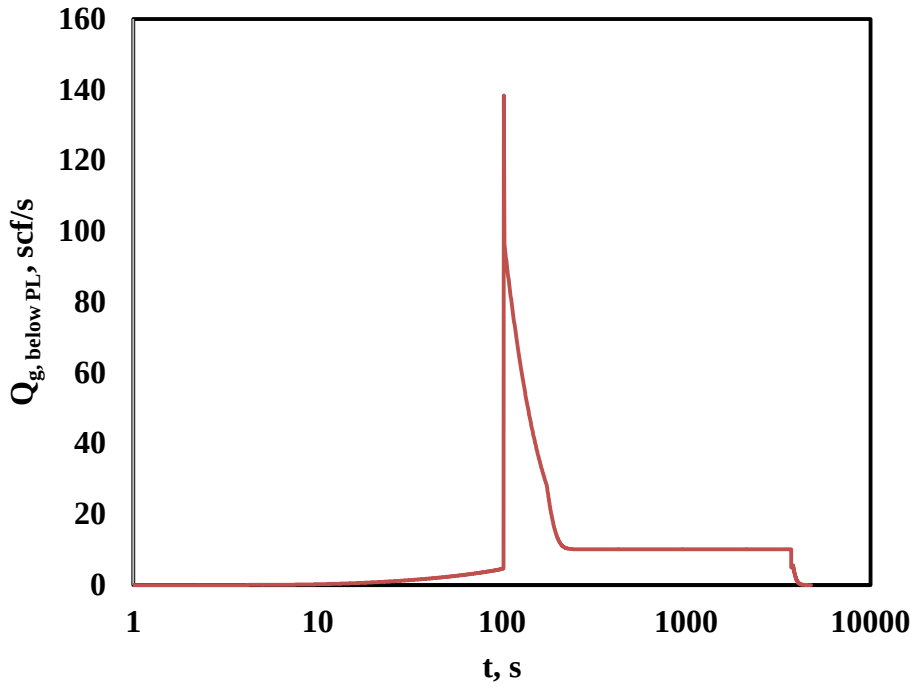

Figure 35: Gas Production Rate below Plunger vs. Time for Entire Cycle (Water Case)

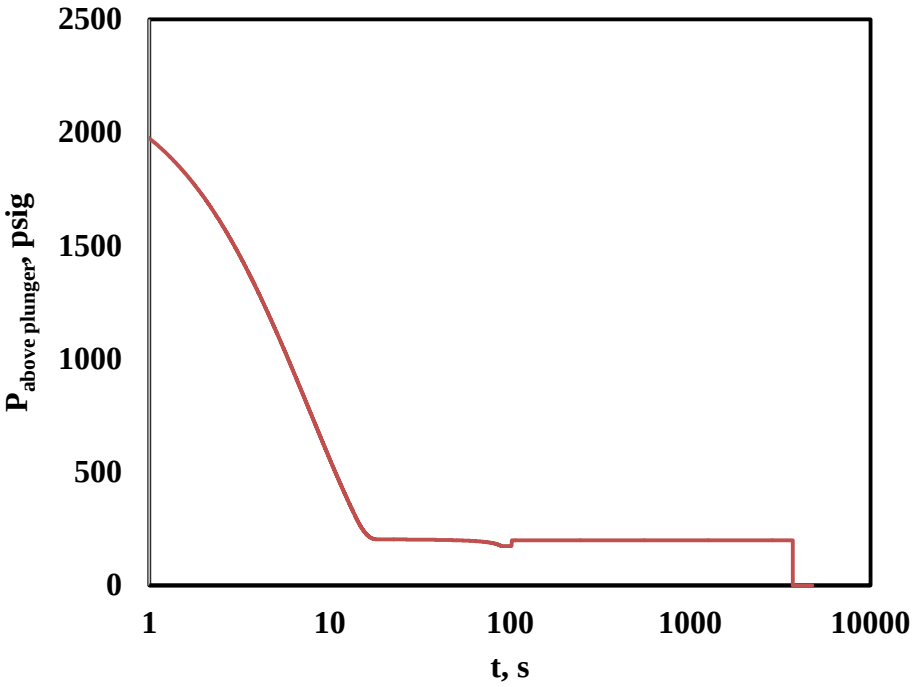

Figure 36: Pressure above Plunger vs. Time for Entire Cycle (Water Case)

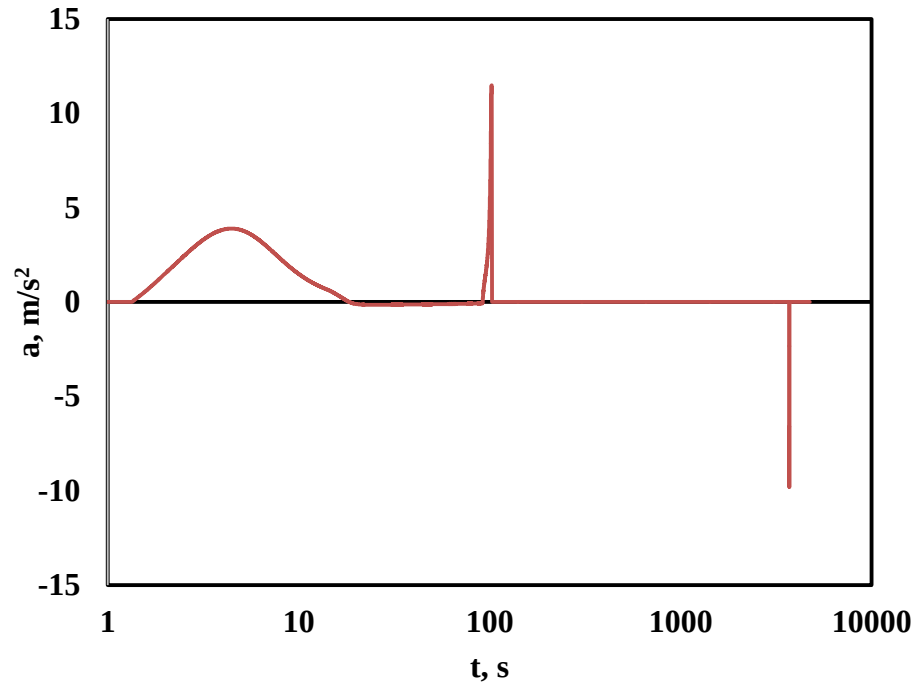

Figure 37: Plunger Acceleration vs. Time for Entire Cycle (Water Case)

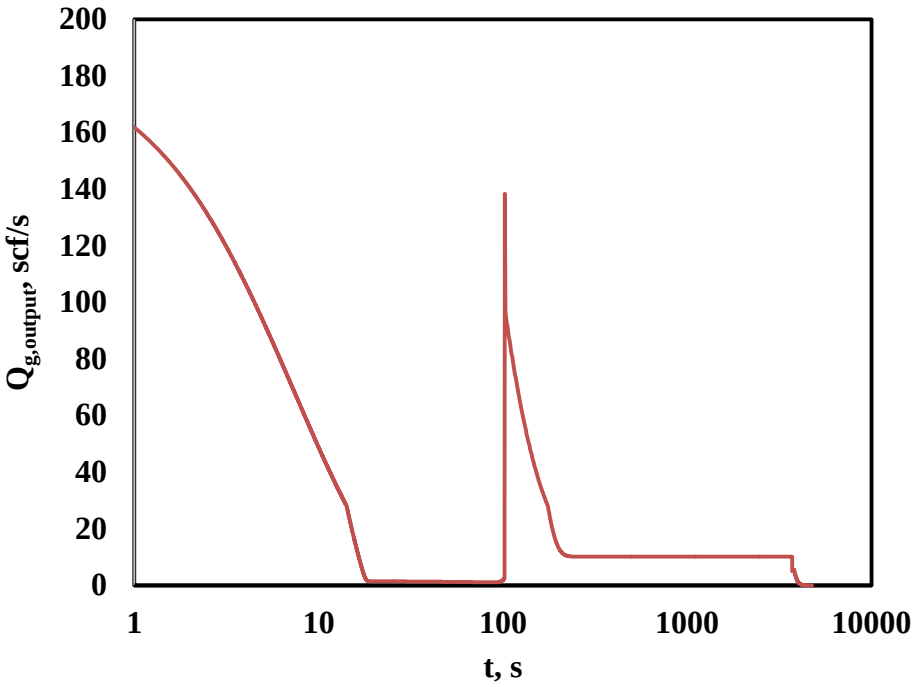

Figure 38: Overall Gas Production Rate vs. Time for Entire Cycle (Water Case)

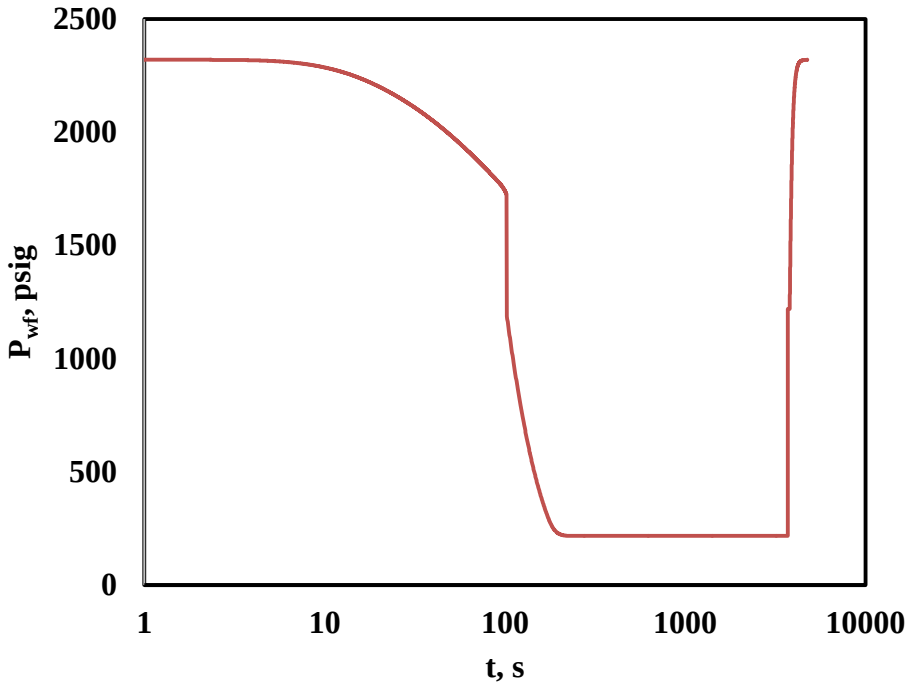

Figure 39: Well Flowing Pressure vs. Time for Entire Cycle (Water Case)

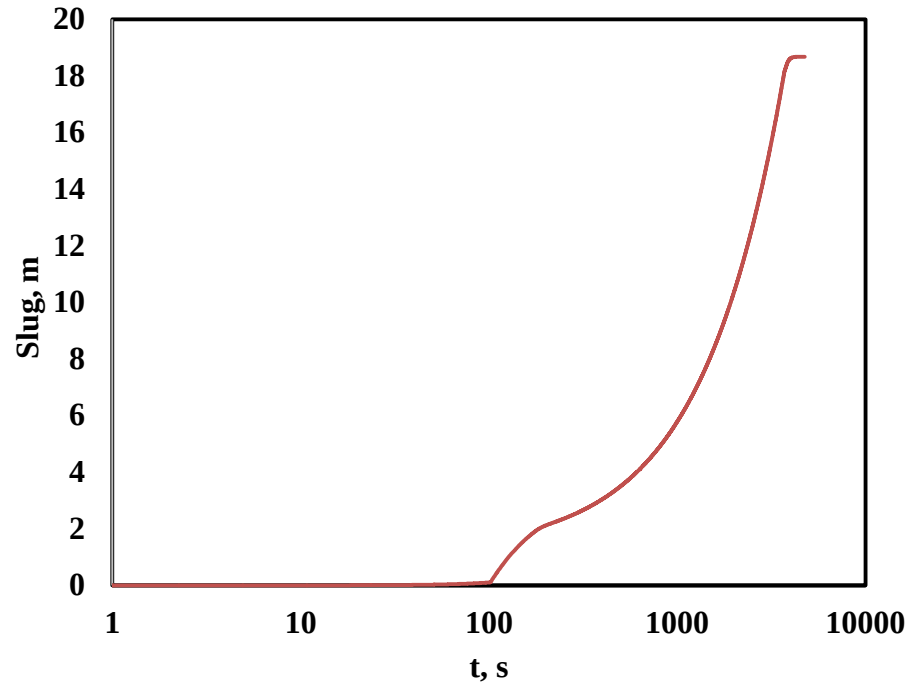

Figure 40: Liquid Slug Accumulations in the Well vs. Time for Entire Cycle (Water Case)

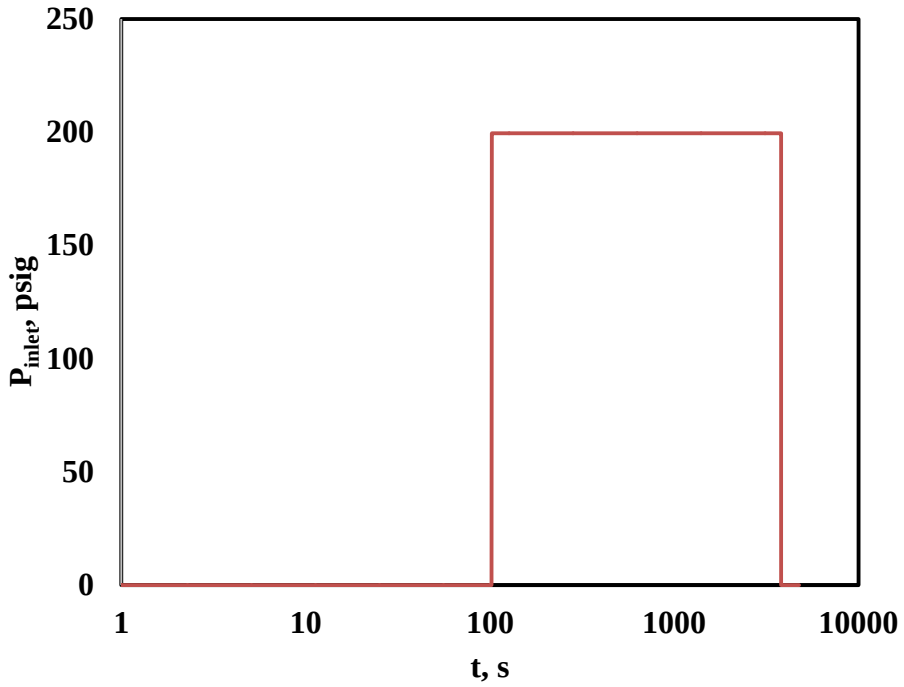

Figure 41: Inlet Pressure vs. Time for Entire Cycle (Water Case)

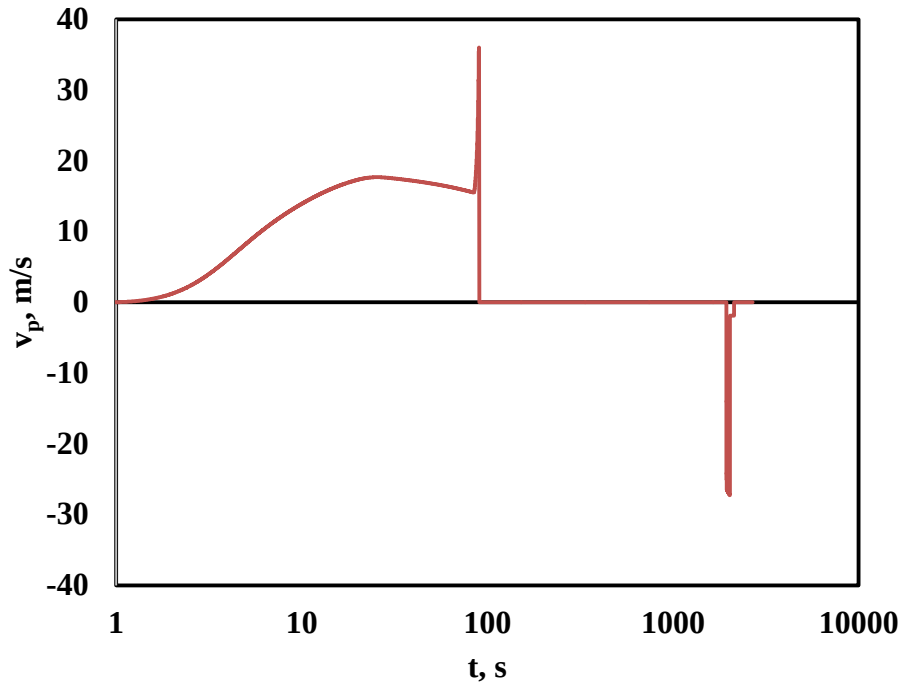

Figure 42: Plunger Velocity vs. Time for Entire Cycle (Oil Case)

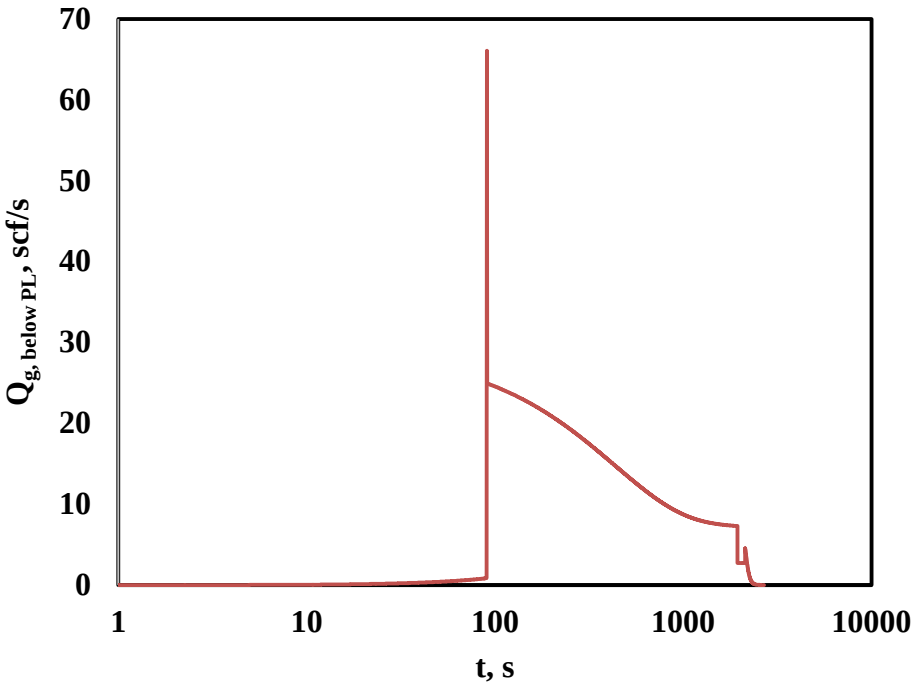

Figure 43: Gas Production Rate below Plunger vs. Time for Entire Cycle (Oil Case)

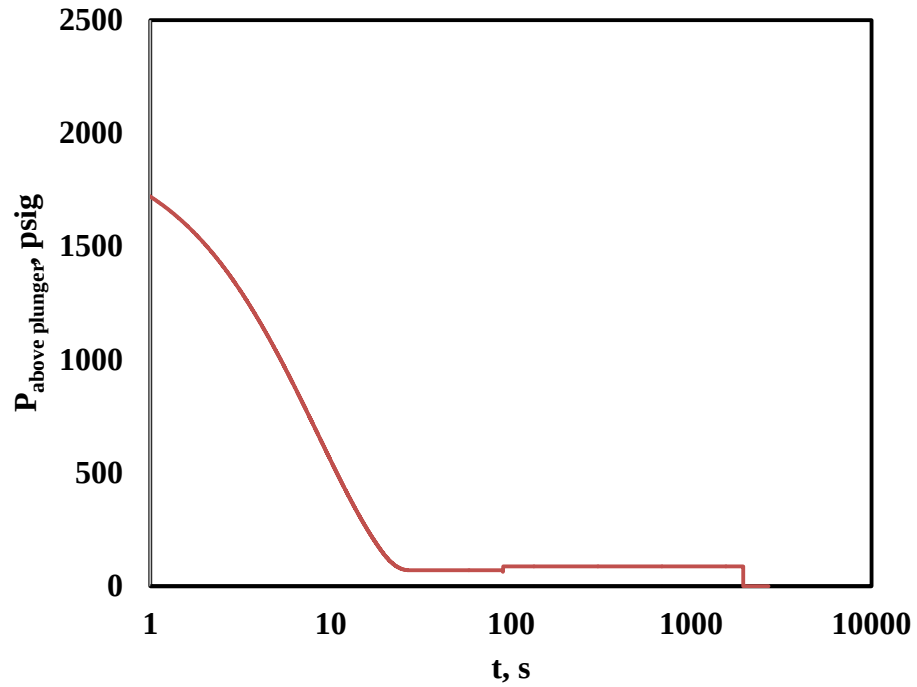

Figure 44: Pressure above Plunger vs. Time for Entire Cycle (Oil Case)

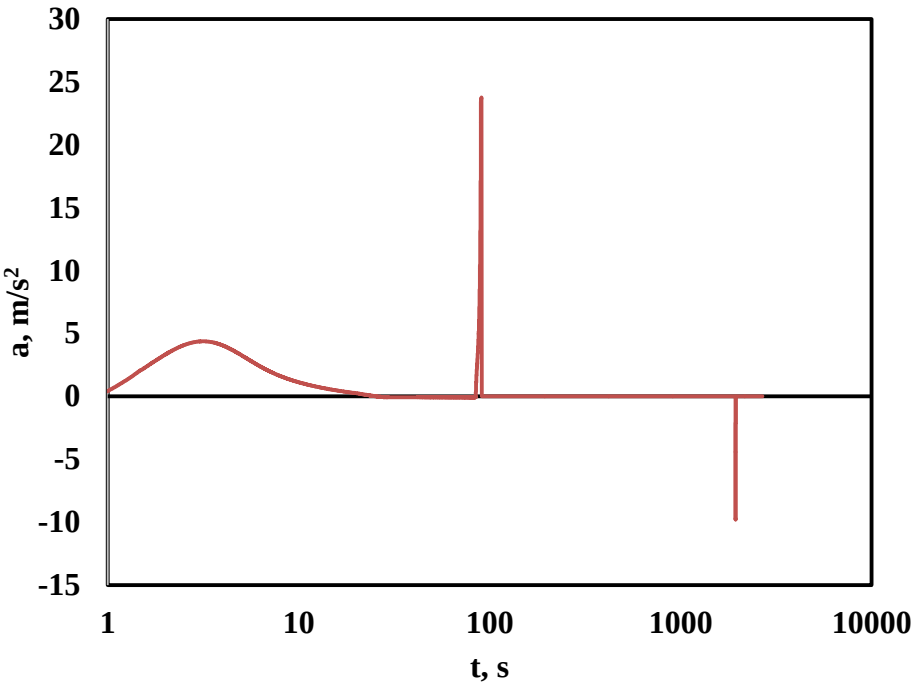

Figure 45: Plunger Acceleration vs. Time for Entire Cycle (Oil Case)

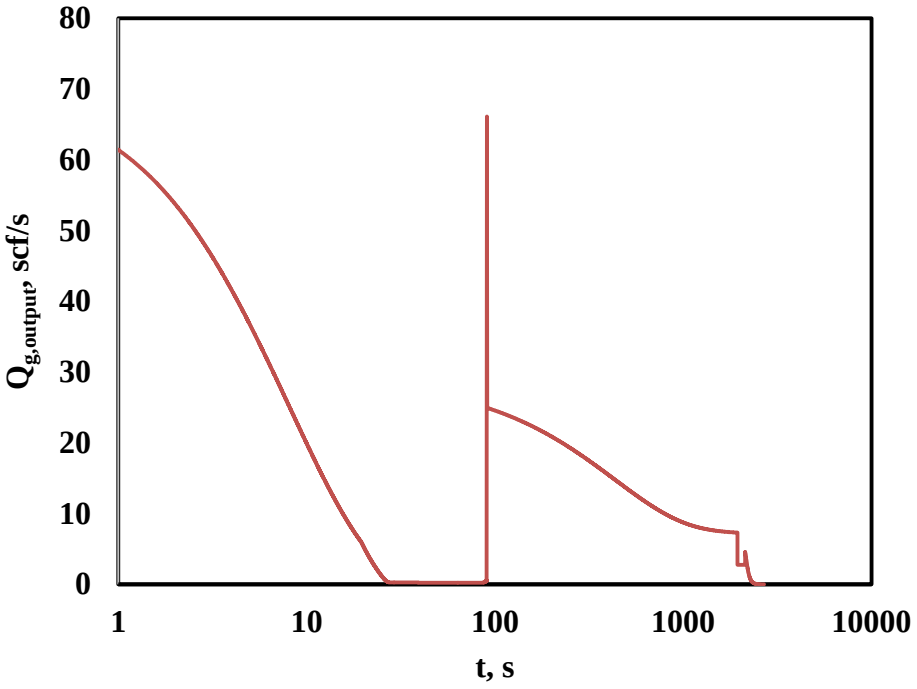

Figure 46: Overall Gas Production Rate vs. Time for Entire Cycle (Oil Case)

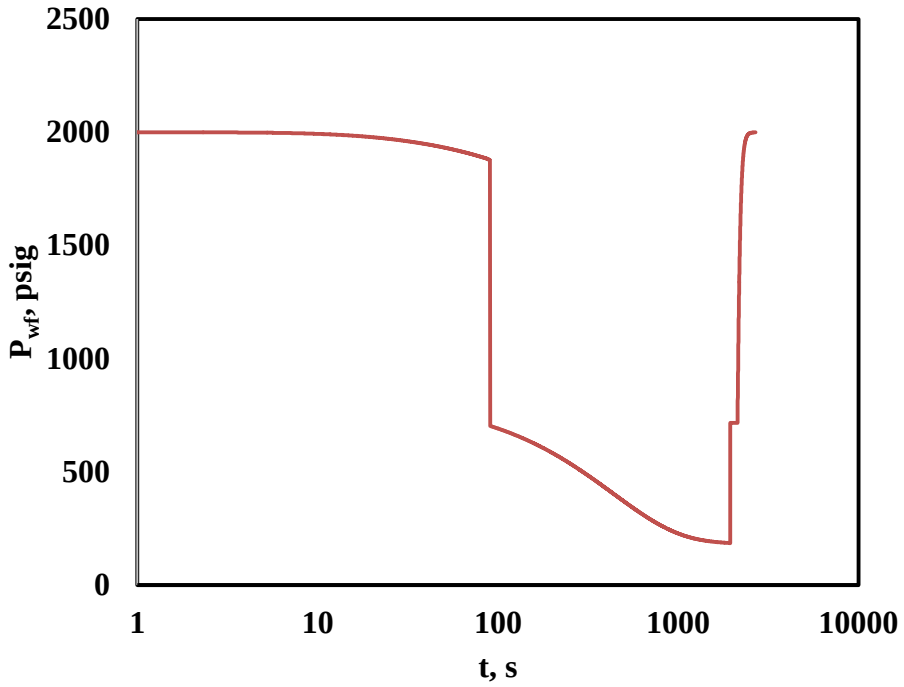

Figure 47: Well Flowing Pressure vs. Time for Entire Cycle (Oil Case)

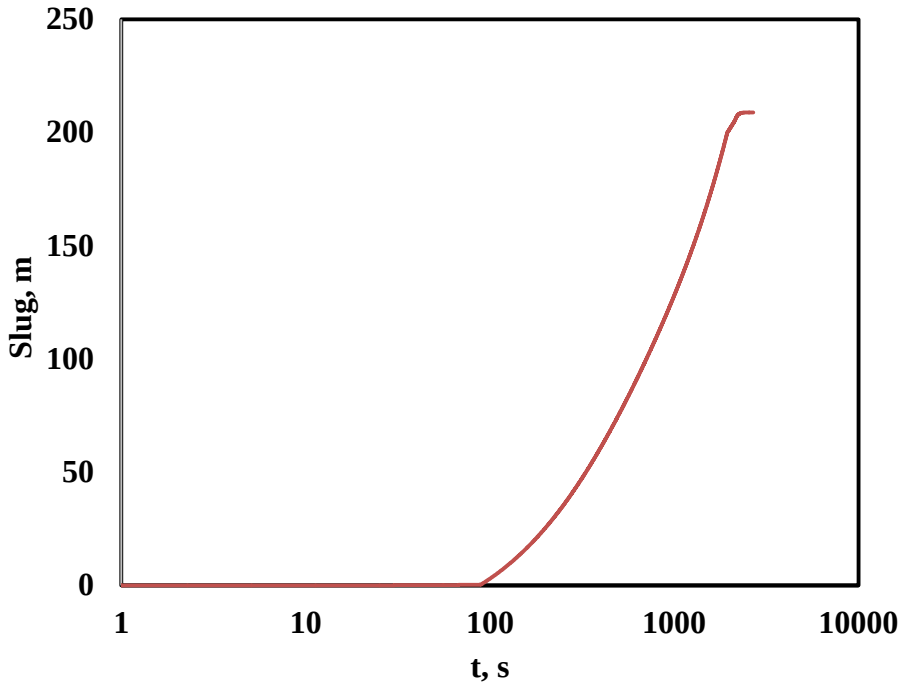

Figure 48: Slug Accumulation vs. Time for Entire Cycle (Oil Case)

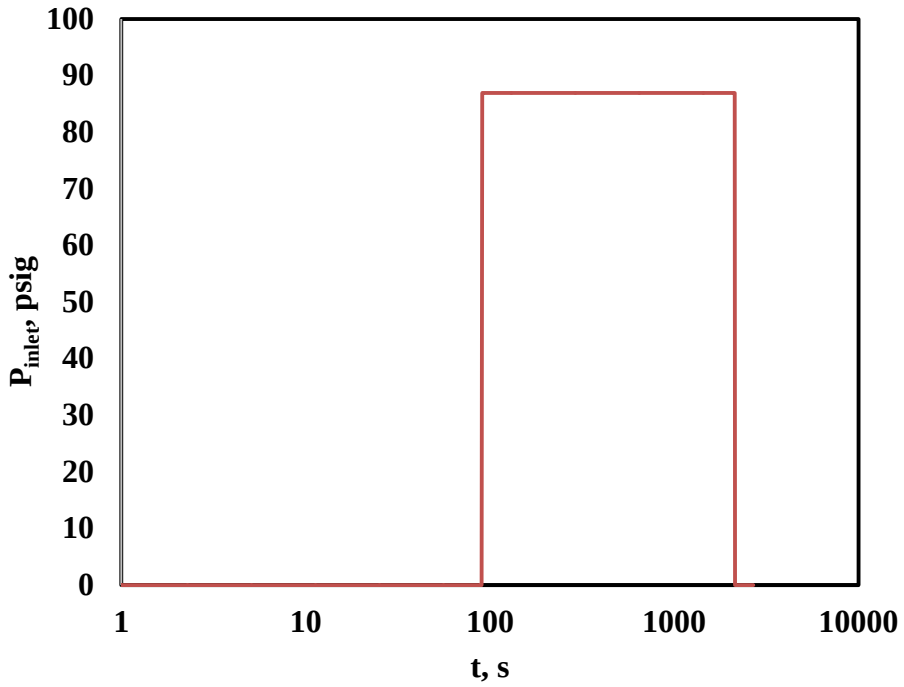

Figure 49: Inlet Pressure vs. Time for Entire Cycle (Oil Case)

APPENDIX B

AUXILIARY EQUATIONS

Supplement equations used in the new plunger lift model are presented below. The Runge-Kutta algorithm is used in the program to solve momentum equations.

Temperature:

$$T = T_{surface} + h\frac{dT}{dL}$$

Reynolds Number:

$$\mathbf{Re} = \frac{\rho v d}{\mu_{SC}}$$

Local sonic velocity:

$$v_{SC} = \sqrt{\frac{1.31P}{\rho_{gas}}}$$

General pressure calculation:

$$P = \rho_g gh + P_{seperator}$$

Gas velocity:

$$v_{gas} = \frac{Q_{gas}}{\frac{\pi}{4}D^2}$$

Gas mass:

$$m_g = 1.29\gamma_{gas}Q_{g,SC}\Delta t$$

Acceleration:

$$a = \frac{F}{m}$$

In-situ gas flow rate:

$$Q_g = Q_{g,SC} \frac{0.1 * 10^{-6} Z}{P} \frac{T}{273.15}$$

Standard gas flow rate:

$$Q_{g,SC} = \frac{v_g A \rho_{gas-insitu}}{1.29 \gamma_{gas}}$$

Friction factor:

$$x_1 = \frac{\varepsilon}{d}$$

$$x_2 = \frac{5.452}{4\mathrm{Re}} \pi d^2$$

$$x_3 = -2\log(x_2 - x_1)$$

When x_1-x_2>,

$$f = \frac{1}{x_3^2}$$

Other conditions:

$$f = \frac{64}{\mathrm{Re}}$$

Pressure loss due to friction:

$$P_f = \frac{f g_{gas} v_g^2}{2d} L$$